Natural Resources Canada
Ressources naturelles Canada

A 3.0 Ga to 2.0 Ga plutonic record on Southampton Island, Nunavut

N. Rayner, M. Sanborn-Barrie, and J. Chakungal

Geological Survey of Canada
Current Research 2013-6

2013

Canada

Geological Survey of Canada
Current Research 2013-6

A 3.0 Ga to 2.0 Ga plutonic record on Southampton Island, Nunavut

N. Rayner, M. Sanborn-Barrie, and J. Chakungal

2013

ISSN 1701-4387
Catalogue No. M44-2013/6E-PDF
ISBN 978-1-100-21685-0
doi:10.4095/292214

A copy of this publication is also available for reference in depository libraries across Canada through access to the Depository Services Program's Web site at http://dsp-psd.pwgsc.gc.ca

This publication is available for free download through GEOSCAN http://geoscan.ess.nrcan.gc.ca

Recommended citation

Rayner, N., Sanborn-Barrie, M., and Chakungal, J., 2013. A 3.0 Ga to 2.0 Ga plutonic record on Southampton Island, Nunavut; Geological Survey of Canada, Current Research 2013-6, 18 p. doi:10.4095/292214

Critical review

B. Davis

Authors

N. Rayner
(Nicole.Rayner@NRCan-RNCan.gc.ca)
M. Sanborn-Barrie
(Mary.Sanborn-Barrie@NRcan-RNCan.gc.ca)
Geological Survey of Canada
601 Booth Street
Ottawa, Ontario
K1A 0E9

J. Chakungal (joyia.chakungal@gmail.com)
Transterritorial Bedrock Mapping & Consulting Inc.,
20 Cranberry Road, Mendenhall Subdivision,
P.O. Box 40105,
Whitehorse, Yukon
Y1A 4Z7

Correction date:

A 3.0 Ga to 2.0 Ga plutonic record on Southampton Island, Nunavut

N. Rayner, M. Sanborn-Barrie, and J. Chakungal

Rayner, N., Sanborn-Barrie, M., and Chakungal, J., 2013. A 3.0 Ga to 2.0 Ga plutonic record on Southampton Island, Nunavut; Geological Survey of Canada, Current Research 2013-6, 18 p. doi:10.4095/292214

Abstract: New U-Pb SHRIMP and ID-TIMS geochronological results have brought to light an extensive Archean history on Southampton Island, Nunavut. The oldest plutonic component documented is a ca. 3.0 Ga anorthositic complex whereas granulite facies tonalite-quartz diorite from two widespread localities have ages of 2.77–2.76 Ga. This implies that a significant proportion of the Precambrian highland of Southampton Island comprises high-grade plutonic rocks dating back to the Mesoarchean. Mylonitic biotite monzogranite yields an age of 2.61 Ga. Gabbroic anorthosite exposed west of the community of Coral Harbour is dated at 2.06 Ga, corresponding in age with rifting prior to the onset of the Trans-Hudson Orogen. Metamorphism related to the Trans-Hudson Orogen is recorded by zircon overgrowths dated between 1.88 Ga and 1.82 Ga in most rocks analyzed.

Résumé : De nouveaux résultats géochronologiques, issus de datations U-Pb à l'aide de la microsonde SHRIMP et d'analyses ID-TIMS (dilution isotopique et spectrométrie de masse à thermoionisation), ont mis en lumière une histoire archéenne de longue durée dans l'île Southampton, au Nunavut. La plus ancienne composante plutonique qui a été documentée est un complexe anorthositique datant d'environ 3,0 Ga, tandis que de la tonalite-diorite quartzique au faciès des granulites provenant de deux localités éloignées a livré des âges de 2,77-2,76 Ga. Cela signifie qu'une importante proportion des hautes terres précambriennes de l'île Southampton est constituée de roches plutoniques à fort degré de métamorphisme qui remontent au Mésoarchéen. Du monzogranite à biotite mylonitique a livré un âge de 2,61 Ga. De l'anorthosite gabbroïque affleurant à l'ouest de la collectivité de Coral Harbour a été datée à 2,06 Ga, ce qui correspond à l'âge du rifting, avant le début de l'orogenèse trans-hudsonienne. Le métamorphisme lié à l'orogenèse trans-hudsonienne se manifeste par des accroissements secondaires de zircon datant de 1,88 à 1,82 Ga dans la plupart des roches analysées.

GEOLOGICAL BACKGROUND

Southampton Island, Nunavut is situated between the Archean-dominated western Churchill Province and the Paleoproterozoic Baffin-Ungava segment of the Trans-Hudson orogen (Fig. 1a). The island exposes a highland of Precambrian basement across much of its eastern half and flat-lying Paleozoic carbonate strata across its western half. The Precambrian basement complex consists predominantly of tonalite-granodiorite-granite gneiss (Fig. 1b) with enclaves and inclusions of mafic-ultramafic-anorthositic plutonic rocks and lesser metasedimentary rocks (Chakungal et al., 2007, 2008; Sanborn-Barrie et al., 2007, 2008, 2009, in press). These strongly foliated to gneissic plutonic rocks range from amphibolite to granulite facies (Berman et al., 2011), and are typically cut by centimetre-wide, concordant monzogranitic veins, contributing to a pervasive lit-par-lit structure. Late-tectonic granitic plutons are small and rare.

Rayner et al. (2011) established the presence of Paleoproterozoic and lesser Archean rocks forming Southampton Island's basement complex. Archean rocks are represented by 2692 ± 6 Ma hornblende-biotite monzogranite in the north, and 2682 ± 17 Ma peraluminous granite that cuts Archean semipelite in the south-central part of the basement complex. Widespread Paleoproterozoic plutonic rocks include 1934 ± 8 Ma quartz porphyry, 1852 ± 8 Ma biotite-magnetite granodiorite, 1842 ± 5 Ma quartz diorite, and 1822 ± 3 Ma syenogranite (Rayner et al., 2011). In situ U-Pb monazite data from metasedimentary rocks constrained penetrative deformation and metamorphism to between 1.88 Ga and 1.82 Ga (Berman et al., 2011). Collectively, these data established profound magmatic and tectonometamorphic reworking of a Neoarchean crustal domain during the Paleoproterozoic, consistent with penetrative involvement in the Trans-Hudson collision between the Rae and Superior cratons.

The initial geochronological study from Southampton Island investigated only a limited number of lithological units, too few to adequately evaluate the extent and relative proportion of Archean versus Paleoproterozoic lithologies (Rayner et al., 2011). In addition, Nd isotopic data reported by Whalen et al. (2011) indicated significant reworking of Mesoarchean crust during the Neoarchean, yet little evidence for rocks of this age were documented. In this report, U-Pb data are presented for five plutonic samples to provide additional age characterization of some of Southampton Island's major map units. These data, in concert with field relationships, structural, geophysical, geochemical, and other isotopic data provide a much more comprehensive foundation upon which tectonic models for this region can be formulated.

ANALYTICAL METHODS

Heavy minerals were separated using standard crushing, grinding and heavy liquid concentration techniques, followed by magnetic sorting of the heavy minerals with a Frantz isodynamic separator. Sensitive high-resolution ion microprobe (SHRIMP) analyses were carried out on four of the five samples discussed herein. Prior to analysis, the internal features of the zircon crystals (zoning, structures, alteration, etc.) were characterized with backscattered electrons (BSE) and/or cathodoluminescence (CL) utilizing a Zeiss Evo scanning electron microscope. SHRIMP analytical procedure and U-Pb calibration details are given in Stern (1997) and Stern and Amelin (2003). The analytical work presented here was collected over three sessions on three separate ion probe epoxy mounts under varying instrumental conditions. Specific analytical details for each sample are given in the footnotes of Tables 1 and 2. A fifth sample was analyzed by isotope dilution–thermal ionization mass spectrometry (ID-TIMS) following the methods described by Parrish et al. (1987). Mass spectrometric data reduction and numerical propagation of analytical uncertainties follow Roddick (1987). Isoplot v. 3.66 (Ludwig, 2003) was used to generate concordia plots and calculate weighted means. All ages quoted in the text are given at the 95% confidence level. The SHRIMP isotopic data are presented in Table 1, whereas ID-TIMS data are presented in Table 2. Isotopic ratios in Table 1 are given at 1σ uncertainty, as are SHRIMP ages. The ID-TIMS ages (Table 2) are reported in the table with 2σ uncertainties.

Trace-element analyses of zircon grains were carried out on one sample (08CYA-M243, IP519) in a separate analytical session. Twenty-six isotopic species were collected, including all the lanthanides, Ti, Y, Ba, Ta, Hf, Th, and U. Abundances were calibrated against standard 6266 that is chemically homogeneous at the millimicron scale (Stern, 2001). Measurement and calibration errors on abundances are typically between 2–5% (1 σ) with the exception of Ba (15–25%), La (20%), and Ta (17%). External uncertainties on the order of 2–5% relating to the standard composition determined by inductively coupled plasma mass spectrometry (unpub. data) are not included. Results are presented in Table 3.

URANIUM-LEAD RESULTS

Sample 08CYA-J148a (z9710) Nalojoaq anorthosite

Along the east coast of Bell Peninsula (Fig. 1b), is a 2 km long, approximately 100 m wide exposure of light grey- to white-weathering anorthosite (J148a). The anorthosite is characterized by strong, straight, shallow-dipping gneissic layering (Fig. 2a) defined by centimetre- to metre-scale segregation of its mafic minerals (biotite±hornblende), and by a

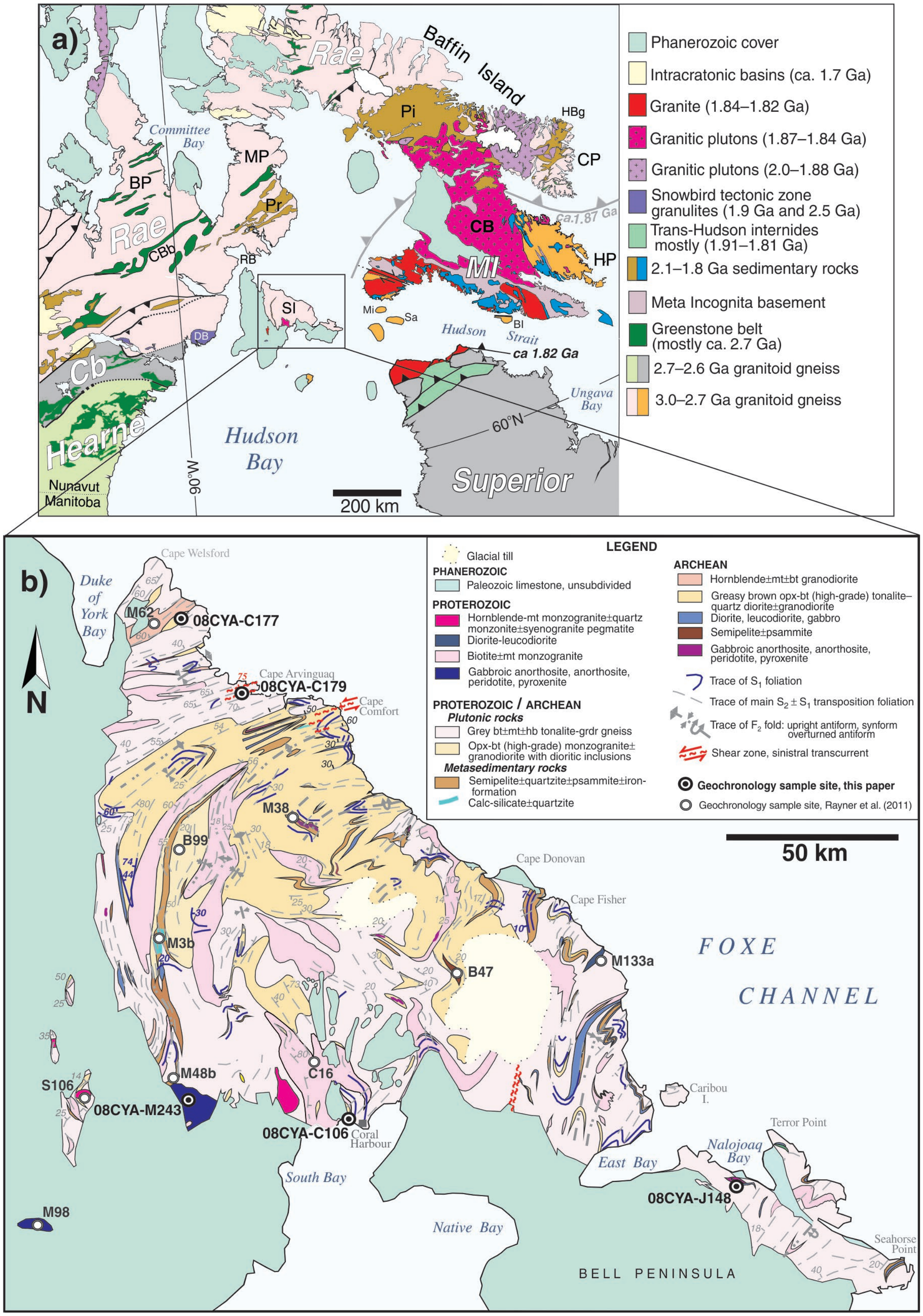

Figure 1. a) Simplified geological map of northeastern Laurentia showing the context of Southampton Island: Abbreviations: BI = Big Island; BP = Boothia Peninsula; Cb = Chesterfield block; CB = Cumberland Batholith, CP = Cumberland Peninsula, CBb = Committee Bay belt; DB = Daly Bay; HBg = Hoare Bay group; HP = Hall Peninsula; Mi = Mill Island; MP = Melville Peninsula; Pi = Piling group; Pr = Penrhyn group; RB = Repulse Bay; Sa = Salisbury Island; SI = Southampton Island. **b)** Simplified bedrock geology of Southampton Island (*after* Sanborn-Barrie et al., in press). Geochronology sample locations for data presented and discussed in this paper are shown with black circles, with sample locations for U-Pb data presented in Rayner et al. (2011) shown with grey circles and abbreviated sample names. mt = magnetite bt = biotite, opx = orthopyroxene, hb = hornlende, grdr = granodiorite.

Table 1. Uranium-lead SHRIMP analytical data.

08CYA-J148A, NAD83, zone 17, 7096299N 495052E																	Apparent ages (Ma)				
Spot name	U (ppm)	Th (ppm)	Th/U	^{206}Pb* (ppm)	^{204}Pb/^{206}Pb	%±	f(206)^{204} %	^{208*}Pb/^{206*}Pb	%±	^{207*}Pb/^{235}U	%±	^{206*}Pb/^{238}U	%±	Corr Coeff	^{207*}Pb/^{206*}Pb	%±	^{206}Pb/^{238}U	±^{206}Pb/^{238}U	^{207}Pb/^{206}Pb	±^{207}Pb/^{206}Pb	Disc. (%)
9710-60.1	20	0.03	0.001	6	6.0E-04	31	1.038	-0.0110	16.0	4.97	3.1	0.3204	1.9	0.598	0.1126	2.49	1792	29	1841	45	3.1
9710-52.2	874	36	0.04	247	7.4E-06	23	0.013	0.0122	2.1	5.13	1.6	0.3287	1.6	0.991	0.1132	0.21	1832	25	1851	4	1.2
9710-68.2	929	42	0.05	238	2.1E-05	24	0.037	0.0133	2.3	4.65	1.6	0.2976	1.6	0.984	0.1133	0.28	1679	23	1854	5	10.7
9710-9.1	2886	226	0.08	877	5.1E-06	32	0.009	0.0235	0.9	5.53	1.5	0.3536	1.5	0.997	0.1134	0.12	1952	26	1855	2	-6.0
9710-6.1	716	41	0.06	198	9.1E-06	121	0.016	0.0180	2.2	5.04	1.6	0.3223	1.6	0.972	0.1135	0.37	1801	24	1855	7	3.4
9710-103.1	881	44	0.05	252	1.7E-05	37	0.029	0.0148	1.9	5.22	1.6	0.3331	1.6	0.988	0.1137	0.25	1853	25	1859	4	0.4
9710-97.1	948	50	0.05	274	1.1E-05	33	0.018	0.0156	1.7	5.27	1.6	0.3363	1.6	0.989	0.1138	0.23	1869	25	1860	4	-0.5
9710-15.1	927	31	0.03	256	5.2E-06	41	0.009	0.0100	2.5	5.04	1.6	0.3210	1.6	0.989	0.1139	0.23	1795	24	1862	4	4.1
9710-4.1	2214	166	0.08	664	9.3E-08	56	0.000	0.0235	0.9	5.48	1.5	0.3489	1.5	0.997	0.1139	0.12	1929	26	1863	2	-4.1
9710-14.1	660	30	0.05	184	2.5E-05	30	0.043	0.0135	2.6	5.10	1.6	0.3242	1.6	0.983	0.1140	0.29	1810	25	1865	5	3.4
9710-77.1	851	36	0.04	242	4.4E-06	171	0.008	0.0133	2.1	5.21	1.6	0.3306	1.6	0.986	0.1142	0.26	1841	25	1867	5	1.6
9710-12.1	822	44	0.05	245	4.1E-06	32	0.007	0.0168	2.0	5.48	1.6	0.3475	1.6	0.989	0.1143	0.23	1923	26	1869	4	-3.3
9710-21.1	995	53	0.05	288	3.7E-06	56	0.006	0.0166	1.7	5.31	1.6	0.3367	1.6	0.990	0.1143	0.22	1871	25	1869	4	-0.1
9710-18.1	797	28	0.04	223	6.1E-06	40	0.011	0.0107	2.4	5.14	1.6	0.3251	1.6	0.987	0.1146	0.25	1815	25	1873	5	3.6
9710-85.1	844	38	0.05	241	7.3E-06	33	0.013	0.0135	3.2	5.25	1.6	0.3323	1.6	0.988	0.1146	0.25	1850	25	1874	4	1.5
9710-10.2	972	51	0.05	253	3.5E-06	47	0.006	0.0174	1.9	4.79	1.6	0.3030	1.5	0.987	0.1147	0.26	1706	23	1875	5	10.2
9710-2.1	37	0.1	0.002	11	1.2E-04	20	0.201	0.0004	19.8	5.30	2.0	0.3350	1.7	0.880	0.1147	0.94	1862	28	1876	17	0.8
9710-96.1	1002	9	0.01	283	7.0E-06	41	0.012	0.0027	4.3	5.23	1.6	0.3295	1.6	0.996	0.1151	0.14	1836	25	1881	3	2.8
9710-100.1	193	0.2	0.001	55	3.1E-05	36	0.053	-0.0004	20.1	5.28	1.6	0.3322	1.6	0.977	0.1153	0.34	1849	25	1885	6	2.2
9710-25.1	116	0.3	0.003	31	1.9E-05	310	0.033	0.0012	18.0	4.95	1.9	0.3101	1.7	0.907	0.1158	0.81	1741	27	1892	15	9.1
9710-65.1	30	---	---	8	3.0E-04	40	0.514	-0.0022	15.0	5.23	2.4	0.3258	1.8	0.739	0.1165	1.60	1818	28	1904	29	5.2
9710-82.1	21	0.02	0.001	6	1.2E-04	62	0.208	0.0045	24.6	5.38	2.5	0.3305	2.1	0.855	0.1181	1.28	1841	34	1928	23	5.2
9710-28.1	277	66	0.25	96	-1.1E-05	21	-0.019	0.0727	1.6	10.32	1.7	0.4030	1.6	0.917	0.1856	0.69	2183	29	2704	11	22.7
9710-20.1	309	62	0.21	131	2.0E-05	52	0.034	0.0581	1.4	13.71	1.7	0.4934	1.7	0.992	0.2015	0.22	2586	37	2838	4	10.8
9710-102.2	320	38	0.12	117	1.8E-05	39	0.031	0.0353	2.0	11.87	1.6	0.4270	1.6	0.985	0.2016	0.28	2292	30	2839	5	22.8
9710-87.1	404	67	0.17	179	5.3E-07	932	0.001	0.0499	1.3	14.37	1.6	0.5162	1.6	0.995	0.2019	0.15	2683	34	2841	2	6.8
9710-79.1	128	28	0.23	56	2.1E-05	108	0.036	0.0638	2.1	14.28	1.6	0.5128	1.6	0.985	0.2019	0.29	2669	35	2841	5	7.4
9710-78.1	503	54	0.11	223	1.7E-05	44	0.029	0.0313	1.5	14.38	1.7	0.5163	1.6	0.894	0.2020	0.78	2683	34	2843	13	6.8
9710-106.1	388	68	0.18	169	5.0E-05	21	0.087	0.0499	1.4	14.35	1.6	0.5089	1.6	0.995	0.2045	0.16	2652	34	2862	3	9.0
9710-102.3	402	56	0.14	135	1.4E-05	52	0.024	0.0391	2.2	11.03	1.6	0.3913	1.6	0.981	0.2046	0.31	2129	28	2863	5	30.0
9710-24.1	234	36	0.16	103	1.9E-05	56	0.033	0.0461	1.7	14.48	1.9	0.5133	1.8	0.982	0.2046	0.35	2671	40	2863	6	8.2
9710-10.4	665	146	0.23	241	1.2E-05	155	0.020	0.0628	1.2	11.93	1.6	0.4222	1.6	0.989	0.2048	0.24	2271	30	2865	4	24.6
9710-36.1	479	25	0.05	212	7.1E-06	194	0.012	0.0149	2.2	14.58	1.6	0.5158	1.6	0.977	0.2051	0.35	2681	35	2867	6	7.9
9710-10.3	468	105	0.23	182	9.8E-06	19	0.017	0.0675	1.2	12.78	1.6	0.4517	1.6	0.991	0.2053	0.22	2403	31	2868	4	19.4
9710-83.1	294	36	0.13	132	2.4E-06	4	0.004	0.0369	1.8	14.86	1.6	0.5227	1.6	0.993	0.2062	0.19	2711	35	2876	3	7.0
9710-26.3	23	10	0.46	9	-1.0E-04	15	-0.178	0.1357	3.7	13.30	2.0	0.4672	1.9	0.945	0.2065	0.65	2471	39	2879	11	17.0
9710-16.1	367	43	0.12	164	3.5E-06	67	0.006	0.0357	1.6	14.89	1.7	0.5205	1.7	0.994	0.2075	0.19	2701	37	2886	3	7.8
9710-10.1	469	103	0.23	219	-3.2E-06	127	-0.006	0.0640	1.0	15.65	1.6	0.5437	1.5	0.997	0.2087	0.12	2799	35	2896	2	4.1
9710-68.1	314	55	0.18	144	4.3E-05	31	0.075	0.0517	1.4	15.49	1.6	0.5356	1.6	0.991	0.2098	0.21	2765	35	2904	3	5.9
9710-35.1	274	67	0.25	112	5.6E-06	72	0.010	0.0725	1.4	13.79	1.6	0.4767	1.6	0.993	0.2098	0.18	2513	33	2904	3	16.2
9710-4.2	371	41	0.12	155	3.1E-06	294	0.005	0.0333	1.9	14.06	1.6	0.4858	1.6	0.989	0.2098	0.23	2552	33	2904	4	14.6
9710-52.1	78	15	0.20	36	7.1E-05	34	0.123	0.0522	2.8	15.49	1.7	0.5345	1.6	0.978	0.2102	0.34	2760	36	2907	6	6.2
9710-102.1	360	41	0.12	174	1.1E-05	30	0.019	0.0339	1.6	16.45	1.6	0.5637	1.6	0.987	0.2117	0.26	2882	37	2918	4	1.5
9710-31.1	344	200	0.60	156	6.4E-05	17	0.111	0.1086	0.9	15.39	1.6	0.5273	1.6	0.995	0.2117	0.16	2730	35	2919	3	7.9
9710-64.1	197	30	0.16	91	2.6E-05	35	0.045	0.0372	2.1	15.66	1.6	0.5350	1.6	0.991	0.2124	0.21	2762	35	2924	3	6.8
9710-23.1	197	24	0.13	88	5.2E-05	25	0.090	0.0347	2.2	15.27	1.6	0.5213	1.6	0.970	0.2124	0.39	2705	35	2924	6	9.2
9710-33.1	146	2	0.02	62	6.3E-05	27	0.109	0.0031	7.0	14.70	1.6	0.4965	1.6	0.971	0.2147	0.39	2599	34	2941	6	14.1
9710-84.4	167	7	0.05	61	6.1E-05	28	0.105	0.0128	7.3	12.60	2.0	0.4225	2.0	0.976	0.2163	0.44	2272	38	2953	7	27.3
9710-26.1	44	19	0.46	21	5.9E-05	33	0.102	0.1302	2.3	16.83	1.7	0.5640	1.6	0.976	0.2165	0.36	2883	37	2955	6	3.0
9710-58.1	47	25	0.54	21	1.9E-04	27	0.336	0.1521	2.2	15.94	1.7	0.5337	1.7	0.958	0.2167	0.50	2757	38	2956	8	8.3
9710-84.2	77	3	0.04	31	6.3E-05	24	0.109	0.0091	7.0	14.18	1.7	0.4743	1.6	0.929	0.2168	0.65	2502	34	2957	10	18.5
9710-26.2	18	6	0.34	7	3.1E-04	24	0.545	0.0899	5.3	13.86	2.1	0.4556	1.9	0.904	0.2207	0.90	2420	38	2986	14	22.7
9710-84.1	34	1	0.04	17	8.2E-05	50	0.142	0.0094	8.1	18.26	1.7	0.5923	1.6	0.964	0.2236	0.45	2999	39	3007	7	0.3

Error in ^{206}Pb/^{238}U calibration 1.5% (included).
Standard error in standard calibration was 0.34% (not included in above errors but required when comparing data from different mounts).
Analytical details: mount IP516, 25 µm spot size, primary beam intensity 12nA O_2^-, 6 scans.

Table 1. (Cont.)

Spot name	U (ppm)	Th (ppm)	Th/U	$^{206}Pb^*$ (ppm)	$^{204}Pb/^{206}Pb$	%±	$f(206)^{204}$ %	$^{208*}Pb/^{206*}Pb$	%±	$^{207*}Pb/^{235}U$	%±	$^{206*}Pb/^{238}U$	%±	Corr Coeff	$^{207*}Pb/^{206*}Pb$	%±	Apparent ages (Ma) $^{206}Pb/^{238}U$	$\pm ^{206}Pb/^{238}U$	$^{207}Pb/^{206}Pb$	$\pm ^{207}Pb/^{206}Pb$	Disc. (%)
08CYA-C177, NAD83, zone 17, 7248878N 342784E																					
9708-39.2	517	56	0.11	156	3.9E-05	57	0.068	0.035	2.1	5.86	1.5	0.3510	1.4	0.967	0.1211	0.37	1939	24	1972	7	1.9
9708-17.1	557	95	0.18	181	-4.9E-06	61	-0.009	0.060	1.3	7.93	1.4	0.3778	1.4	0.988	0.1522	0.21	2066	25	2371	4	15.0
9708-83.1	336	102	0.31	133	8.8E-05	24	0.152	0.082	1.4	10.00	1.5	0.4598	1.4	0.977	0.1577	0.31	2439	29	2432	5	-0.4
9708-88.1	638	142	0.23	248	3.8E-06	29	0.007	0.069	1.0	10.44	1.4	0.4531	1.4	0.993	0.1671	0.17	2409	28	2529	3	5.7
9708-71.1	329	61	0.19	133	2.0E-05	64	0.034	0.060	1.6	11.36	1.4	0.4697	1.4	0.984	0.1754	0.26	2482	29	2610	4	5.9
9708-63.1	366	129	0.36	148	4.9E-05	25	0.085	0.100	1.2	11.56	1.5	0.4708	1.4	0.985	0.1780	0.25	2487	30	2635	4	6.8
9708-82.1	567	223	0.41	236	2.0E-07	5244	0.000	0.116	0.8	12.16	1.4	0.4841	1.4	0.991	0.1821	0.19	2545	29	2672	3	5.7
9708-69.1	374	129	0.36	166	-1.8E-08	9999	0.000	0.100	1.1	13.26	1.4	0.5159	1.4	0.989	0.1865	0.21	2682	31	2711	3	1.3
9708-78.1	412	177	0.44	188	4.1E-06	332	0.007	0.124	0.9	13.77	1.4	0.5325	1.4	0.989	0.1875	0.21	2752	32	2720	3	-1.4
9708-10.1	393	149	0.39	171	1.0E-05	44	0.018	0.108	1.0	13.13	1.4	0.5065	1.4	0.989	0.1880	0.21	2642	31	2724	3	3.7
9708-73.1	161	34	0.22	72	3.9E-05	126	0.068	0.064	2.0	13.71	1.5	0.5250	1.5	0.957	0.1893	0.45	2720	33	2737	7	0.7
9708-39.1	391	154	0.41	167	1.2E-05	23	0.021	0.114	1.0	12.98	1.4	0.4962	1.4	0.989	0.1897	0.21	2598	30	2739	4	6.3
9708-03.1	284	61	0.22	128	2.0E-05	34	0.035	0.060	1.7	13.73	1.5	0.5244	1.4	0.968	0.1898	0.37	2718	32	2741	6	1.0
9708-75.1	386	81	0.22	178	5.8E-06	189	0.010	0.057	2.1	14.18	1.4	0.5374	1.4	0.989	0.1914	0.21	2772	32	2755	4	-0.8
9708-30.1	372	137	0.38	162	8.1E-06	34	0.014	0.105	1.1	13.44	1.4	0.5081	1.4	0.989	0.1918	0.22	2649	31	2758	4	4.8
9708-04.1	324	87	0.28	144	6.7E-06	30	0.012	0.077	1.3	13.72	1.4	0.5179	1.4	0.988	0.1921	0.22	2690	31	2761	4	3.1
9708-68.1	130	36	0.29	58	4.1E-06	952	0.007	0.078	2.0	13.86	1.5	0.5229	1.5	0.963	0.1922	0.42	2712	33	2761	7	2.2
9708-95.1	367	144	0.40	172	7.6E-06	175	0.013	0.111	1.0	14.47	1.4	0.5436	1.4	0.988	0.1930	0.22	2798	32	2768	4	-1.3
9708-90.1	314	124	0.41	149	6.5E-06	31	0.011	0.114	1.0	14.72	1.4	0.5523	1.4	0.989	0.1934	0.21	2835	33	2771	3	-2.8
9708-79.1	311	118	0.39	144	2.4E-04	11	0.413	0.109	1.1	14.35	1.4	0.5373	1.4	0.982	0.1936	0.27	2772	32	2773	4	0.1
9708-91.1	570	242	0.44	268	-1.3E-07	5221	0.000	0.125	0.8	14.63	1.4	0.5474	1.4	0.993	0.1938	0.16	2814	32	2774	3	-1.8

Error in $^{206}Pb/^{238}U$ calibration 1.37% (included).
Standard error in standard calibration was 0.34% (not included in above errors, but required when comparing data from different mounts).
Analytical details: mount IP512, 25 µm spot size, primary beam intensity 10nA O_2-, 6 scans

Notes (*see* Stern, 1997):
Spot name follows the convention x-y.z; where x = sample number, y = grain number, and z = spot number.
--- below detection
Corr Coeff = correlation coefficient
Uncertainties reported at 1σ and are calculated by using SQUID 2.23.08.10.21, rev. 21 Oct 2008.
$f206^{204}$ refers to mole per cent of total ^{206}Pb that is due to common Pb, calculated using the ^{204}Pb method; common Pb composition used is the surface blank (4/6: 0.05770; 7/6: 0.89500; 8/6: 2.13840).
* Refers to radiogenic Pb (corrected for common Pb).
Discordance relative to origin = 100 * ((207/206 age -206/238 age)/($^{207}Pb/^{206}Pb$ age)).
Calibration standard 6266; U = 910 ppm; age = 559 Ma; $^{206}Pb/^{238}U$ = 0.09059.
Error in $^{206}Pb/^{238}U$ calibration 1.2% (included).
Standard error in standard calibration was 0.29% (not included in above errors, but required when comparing data from different mounts).
Analytical details: mount IP519, 25 µm spot size, primary beam intensity 14nA O_2-, 6 scans.

Table 1. (Cont.)

Spot name	U (ppm)	Th (ppm)	Th/U	$^{206}Pb^*$ (ppm)	$^{204}Pb/^{206}Pb$	%±	$f(206)^{204}$ %	$^{208*}Pb/^{206*}Pb$	%±	$^{207*}Pb/^{235}U$	%±	$^{206*}Pb/^{238}U$	%±	Corr Coeff	$^{207*}Pb/^{206*}Pb$	%±	Apparent ages (Ma) $^{206}Pb/^{238}U$	$\pm^{206}Pb/^{238}U$	$^{207}Pb/^{206}Pb$	$\pm^{207}Pb/^{206}Pb$	Disc. (%)
08CYA-C106, NAD83, zone 17, 7114574N 389628E																					
9707-105.1	832	282	0.35	242	2.9E-05	27	0.050	0.101	0.9	5.20	1.4	0.3392	1.4	0.986	0.111	0.24	1883	23	1819	4	-4.0
9707-59.1	994	22	0.02	359	1.2E-04	12	0.201	0.003	3.0	7.00	1.4	0.4201	1.4	0.964	0.121	0.39	2261	27	1968	7	-17.7
9707-116.1	107	114	1.10	44	-2.7E-05	47	-0.047	0.316	1.1	11.68	1.5	0.4795	1.5	0.957	0.177	0.45	2525	31	2622	7	4.5
9707-76.1	144	187	1.34	62	8.5E-05	23	0.147	0.387	0.8	12.34	1.5	0.4974	1.5	0.976	0.180	0.33	2603	31	2652	5	2.3
9707-63.1	1274	62	0.05	597	2.5E-06	30	0.004	0.014	1.3	13.66	1.4	0.5458	1.4	0.997	0.182	0.12	2808	32	2667	2	-6.5
9707-111.1	123	114	0.96	52	2.0E-05	25	0.034	0.273	1.0	12.35	1.5	0.4935	1.5	0.976	0.182	0.33	2586	31	2667	5	3.7
9707-36.1	633	141	0.23	296	2.4E-05	39	0.042	0.064	0.9	13.72	1.4	0.5447	1.4	0.994	0.183	0.16	2803	32	2677	3	-5.8
9707-32.1	753	36	0.05	333	6.9E-06	117	0.012	0.014	2.0	13.02	1.5	0.5147	1.4	0.946	0.183	0.48	2677	31	2684	8	0.3
9707-77.1	1356	341	0.26	598	2.3E-06	62	0.004	0.074	0.6	13.09	1.4	0.5134	1.4	0.998	0.185	0.10	2671	30	2698	2	1.2
9707-117.1	322	165	0.53	145	-2.7E-06	54	-0.005	0.152	0.8	13.38	1.5	0.5235	1.4	0.943	0.185	0.50	2714	31	2702	8	-0.5
9707-104.1	611	160	0.27	281	-9.9E-07	421	-0.002	0.077	0.8	13.71	1.4	0.5353	1.4	0.995	0.186	0.14	2764	31	2704	2	-2.7
9707-74.1	350	92	0.27	157	8.6E-06	36	0.015	0.075	1.1	13.42	1.4	0.5222	1.4	0.992	0.186	0.18	2708	31	2711	3	0.1
9707-101.1	141	138	1.01	62	1.4E-05	29	0.023	0.292	0.9	13.21	1.7	0.5131	1.5	0.865	0.187	0.84	2670	32	2714	14	2.0
9707-23.2	149	129	0.89	61	5.6E-05	37	0.097	0.248	1.8	12.16	1.5	0.4721	1.5	0.968	0.187	0.38	2493	31	2714	6	9.8
9707-19.2	450	105	0.24	190	1.6E-05	15	0.028	0.068	1.1	12.76	1.4	0.4916	1.4	0.989	0.188	0.21	2577	30	2727	3	6.7
9707-11.2	533	100	0.19	250	1.1E-05	32	0.019	0.055	1.0	14.16	1.4	0.5453	1.4	0.995	0.188	0.14	2806	32	2728	2	-3.5
9707-38.2	97	120	1.28	43	2.3E-06	2087	0.004	0.363	1.0	13.56	1.6	0.5208	1.5	0.952	0.189	0.48	2703	33	2732	8	1.3
9707-08.1	101	136	1.39	45	-1.7E-05	90	-0.029	0.386	1.0	13.78	1.6	0.5248	1.5	0.968	0.190	0.39	2719	34	2746	6	1.2
9707-107.1	634	167	0.27	292	1.0E-05	86	0.018	0.076	0.8	14.10	1.4	0.5354	1.4	0.975	0.191	0.31	2764	31	2751	5	-0.6
9707-65.1	161	233	1.49	76	-8.8E-06	34	-0.015	0.421	0.7	14.41	1.5	0.5457	1.4	0.984	0.192	0.26	2807	33	2756	4	-2.3
9707-118.1	426	85	0.21	200	-2.7E-06	37	-0.005	0.059	1.1	14.42	1.4	0.5459	1.4	0.994	0.192	0.16	2808	32	2756	3	-2.3
9707-64.1	72	5	0.08	33	-3.6E-05	54	-0.063	0.022	4.9	14.00	1.8	0.5297	1.7	0.969	0.192	0.44	2740	39	2757	7	0.7
9707-38.1	1137	74	0.07	528	4.7E-06	33	0.008	0.019	1.2	14.33	1.4	0.5402	1.4	0.994	0.192	0.15	2784	31	2763	3	-1.0
9707-27.1	129	79	0.64	56	1.8E-05	66	0.030	0.182	1.2	13.39	1.5	0.5047	1.5	0.967	0.192	0.38	2634	32	2763	6	5.7
9707-11.1	952	131	0.14	449	5.6E-06	69	0.010	0.038	1.2	15.06	1.5	0.5483	1.5	0.997	0.199	0.11	2818	33	2820	2	0.1
9707-73.1	118	133	1.17	57	6.6E-06	335	0.011	0.318	0.9	16.51	1.5	0.5677	1.5	0.977	0.211	0.32	2898	34	2913	5	0.6
9707-110.1	490	228	0.48	242	1.3E-07	2334	0.000	0.137	1.1	16.76	1.4	0.5753	1.4	0.995	0.211	0.15	2930	33	2916	2	-0.6
9707-40.1	104	116	1.14	53	2.7E-05	51	0.048	0.325	0.9	18.05	1.5	0.5862	1.5	0.979	0.223	0.31	2974	35	3005	5	1.3
9707-78.1	98	83	0.88	49	3.9E-06	907	0.007	0.236	1.9	18.31	1.7	0.5862	1.5	0.885	0.227	0.78	2974	36	3028	13	2.2
9707-19.1	1909	706	0.38	1070	1.5E-06	138	0.003	0.106	0.4	21.98	1.6	0.6527	1.5	0.956	0.244	0.47	3239	39	3148	7	-3.7
9707-23.1	804	493	0.63	437	3.0E-06	32	0.005	0.175	0.5	21.79	1.4	0.6319	1.4	0.997	0.250	0.11	3157	35	3185	2	1.1

Error in $^{206}Pb/^{238}U$ calibration 1.37% (included).
Standard error in standard calibration was 0.34% (not included in above errors but required when comparing data from different mounts).
Analytical details: mount IP512, 25 µm spot size, primary beam intensity 10nA O_2^-, 6 scans.

Table 1. (Cont.)

	08CYA-M243A, NAD83, zone 17, 7118161N 346478E																Apparent ages (Ma)				
Spot name	U (ppm)	Th (ppm)	$\frac{Th}{U}$	$^{206}Pb^*$ (ppm)	$\frac{^{204}Pb}{^{206}Pb}$	%±	$f(206)^{204}$ %	$\frac{^{208*}Pb}{^{206*}Pb}$	%±	$\frac{^{207*}Pb}{^{235}U}$	%±	$\frac{^{206*}Pb}{^{238}U}$	%±	Corr Coeff	$\frac{^{207*}Pb}{^{206*}Pb}$	%±	$\frac{^{206}Pb}{^{238}U}$	$\pm\frac{^{206}Pb}{^{238}U}$	$\frac{^{207}Pb}{^{206}Pb}$	$\pm\frac{^{207}Pb}{^{206}Pb}$	Disc. (%)
9711-96.2	125	122	1.01	37	1.0E-32	100	0.000	0.305	1.4	5.92	1.8	0.3480	1.3	0.742	0.1233	1.17	1925	22	2004	21	4.6
9711-91.1	140	133	0.98	44	5.9E-05	58	0.101	0.289	1.3	6.23	1.4	0.3641	1.3	0.906	0.1242	0.60	2002	22	2017	11	0.9
9711-29.1	131	141	1.12	41	6.2E-05	18	0.108	0.327	1.3	6.33	1.4	0.3687	1.3	0.930	0.1244	0.51	2023	23	2021	9	-0.2
9711-96.1	205	212	1.07	64	1.9E-05	33	0.032	0.317	1.0	6.25	1.4	0.3633	1.3	0.956	0.1247	0.40	1998	22	2025	7	1.6
9711-27.1	198	164	0.86	64	1.5E-05	182	0.026	0.255	1.1	6.50	1.4	0.3761	1.3	0.941	0.1254	0.47	2058	23	2034	8	-1.4
9711-31.1	98	94	0.99	31	8.2E-05	34	0.142	0.289	1.6	6.45	1.5	0.3734	1.3	0.892	0.1254	0.67	2045	23	2034	12	-0.6
9711-33.1	81	78	1.00	26	7.1E-05	27	0.123	0.293	1.7	6.52	1.5	0.3756	1.3	0.892	0.1258	0.67	2056	23	2040	12	-0.9
9711-74.2	67	51	0.79	25	2.2E-04	24	0.384	0.237	1.7	7.72	1.6	0.4449	1.3	0.855	0.1259	0.82	2372	27	2041	14	-19.4
9711-92.1	188	237	1.31	60	3.0E-05	38	0.052	0.380	0.9	6.48	1.3	0.3731	1.3	0.953	0.1260	0.41	2044	22	2043	7	-0.1
9711-43.1	78	71	0.94	25	2.1E-05	3	0.036	0.282	1.8	6.49	1.5	0.3734	1.3	0.894	0.1260	0.67	2046	24	2043	12	-0.1
9711-72.1	149	147	1.02	49	2.8E-05	131	0.049	0.305	1.1	6.68	1.4	0.3838	1.3	0.911	0.1262	0.58	2094	23	2045	10	-2.8
9711-65.1	162	209	1.33	56	3.0E-05	21	0.052	0.397	0.9	7.01	1.3	0.4024	1.3	0.959	0.1263	0.38	2180	24	2047	7	-7.7
9711-3.1	182	274	1.55	57	9.1E-06	59	0.016	0.465	0.9	6.36	1.6	0.3655	1.5	0.941	0.1263	0.54	2008	26	2047	9	2.2
9711-15.1	87	86	1.02	29	9.0E-05	58	0.156	0.307	1.6	6.67	1.6	0.3828	1.4	0.856	0.1263	0.82	2089	24	2047	15	-2.4
9711-92.2	100	93	0.97	29	1.0E-04	42	0.173	0.267	2.0	5.97	1.6	0.3428	1.4	0.853	0.1263	0.84	1900	23	2047	15	8.3
9711-33.2	75	81	1.12	24	1.4E-04	35	0.243	0.320	1.8	6.38	1.6	0.3661	1.3	0.837	0.1264	0.88	2011	23	2049	16	2.2
9711-26.1	121	153	1.31	39	1.0E-32	100	0.000	0.383	1.2	6.56	1.4	0.3762	1.3	0.901	0.1264	0.63	2059	23	2049	11	-0.6
9711-69.1	111	120	1.12	35	3.0E-05	119	0.052	0.336	1.3	6.44	1.6	0.3692	1.5	0.915	0.1265	0.65	2026	26	2050	12	1.4
9711-79.1	311	572	1.90	98	1.9E-05	38	0.033	0.563	0.6	6.42	1.4	0.3664	1.4	0.973	0.1270	0.33	2012	24	2057	6	2.5
9711-84.1	124	136	1.13	40	4.9E-05	21	0.085	0.335	1.3	6.55	1.4	0.3733	1.3	0.931	0.1272	0.51	2045	23	2060	9	0.9
9711-81.1	80	74	0.96	26	4.2E-05	96	0.073	0.275	1.8	6.60	1.5	0.3762	1.3	0.867	0.1273	0.77	2059	24	2061	14	0.1
9711-47.1	101	94	0.96	33	3.8E-05	21	0.066	0.281	1.5	6.63	1.4	0.3779	1.3	0.923	0.1273	0.55	2066	23	2061	10	-0.3
9711-77.1	103	114	1.14	33	4.0E-5	50	0.070	0.345	1.4	6.56	1.4	0.3738	1.3	0.909	0.1273	0.60	2047	23	2061	11	0.8
9711-91.2	191	169	0.91	60	3.3E-5	33	0.058	0.268	1.1	6.44	1.4	0.3671	1.3	0.952	0.1273	0.42	2016	23	2061	7	2.6
9711-63.1	132	145	1.13	43	5.9E-5	18	0.102	0.337	1.2	6.66	1.8	0.3792	1.7	0.961	0.1273	0.49	2072	30	2061	9	-0.6
9711-85.1	86	89	1.08	27	-4.2E-5	59	-0.074	0.315	1.6	6.52	1.5	0.3712	1.3	0.893	0.1274	0.67	2035	23	2062	12	1.6
9711-29.2	187	189	1.04	55	2.6E-5	85	0.044	0.313	1.3	5.99	1.4	0.3403	1.3	0.922	0.1276	0.54	1888	21	2065	10	9.9
9711-22.1	103	107	1.07	33	3.6E-5	24	0.062	0.323	1.4	6.51	1.4	0.3700	1.3	0.921	0.1277	0.56	2029	23	2066	10	2.1
9711-3.2	149	202	1.40	47	1.0E-32	100	0.000	0.397	1.1	6.42	1.4	0.3647	1.3	0.936	0.1277	0.49	2005	22	2067	9	3.5
9711-78.1	112	139	1.29	36	1.0E-32	100	0.000	0.380	1.2	6.54	1.4	0.3703	1.3	0.935	0.1281	0.51	2031	23	2072	9	2.3
9711-37.1	108	105	1.00	35	1.9E-5	111	0.033	0.298	1.4	6.64	1.4	0.3759	1.3	0.918	0.1282	0.57	2057	23	2074	10	0.9
9711-78.2	97	111	1.19	29	5.6E-5	29	0.098	0.343	1.8	6.17	1.5	0.3488	1.3	0.875	0.1283	0.74	1929	22	2075	13	8.1
9711-20.1	108	139	1.33	35	-3.9E-5	87	-0.068	0.382	1.3	6.61	1.5	0.3735	1.3	0.896	0.1284	0.65	2046	23	2076	11	1.7
9711-97.2	97	92	0.98	30	-6.5E-5	2	-0.112	0.290	1.9	6.35	1.5	0.3590	1.3	0.884	0.1284	0.71	1978	23	2076	12	5.5
9711-72.2	120	134	1.15	37	3.9E-5	33	0.068	0.330	1.5	6.34	1.4	0.3580	1.3	0.913	0.1285	0.58	1973	22	2078	10	5.9
9711-34.1	91	64	0.73	30	3.1E-5	2	0.054	0.209	1.8	6.77	1.4	0.3819	1.3	0.917	0.1286	0.57	2085	24	2079	10	-0.4
9711-8.1	56	56	1.03	19	-5.6E-5	188	-0.098	0.307	1.9	6.84	2.0	0.3850	1.4	0.699	0.1289	1.41	2100	25	2083	25	-1.0
9711-97.1	91	90	1.03	29	-1.3E-5	95	-0.023	0.304	1.6	6.69	1.4	0.3750	1.3	0.911	0.1294	0.60	2053	23	2090	10	2.0
9711-87.1	87	91	1.09	28	-3.6E-5	86	-0.062	0.318	1.6	6.67	1.5	0.3702	1.3	0.891	0.1307	0.67	2030	23	2108	12	4.3
9711-61.1	125	131	1.09	42	1.0E-32	100	0.000	0.308	1.3	7.12	1.5	0.3916	1.4	0.947	0.1319	0.47	2130	25	2124	8	-0.4
9711-95.2	89	86	0.99	28	1.0E-32	100	0.000	0.278	2.1	6.74	1.7	0.3644	1.5	0.898	0.1342	0.74	2003	26	2154	13	8.1
9711-61.2	126	94	0.77	42	-2.4E-6	553	-0.004	0.227	1.6	7.24	1.5	0.3899	1.5	0.943	0.1348	0.52	2122	26	2161	9	2.1
9711-51.1	115	136	1.23	40	1.6E-5	176	0.027	0.354	1.2	7.75	1.4	0.4047	1.3	0.924	0.1389	0.54	2191	24	2213	9	1.2
9711-87.2	92	89	1.00	31	8.9E-5	30	0.155	0.295	1.7	7.46	1.7	0.3884	1.4	0.791	0.1394	1.06	2116	25	2219	18	5.5
9711-136.1	63	61	1.00	22	-3.8E-5	148	-0.065	0.307	1.9	7.72	1.6	0.3995	1.4	0.847	0.1401	0.86	2167	25	2228	15	3.3
9711-148.1	61	64	1.09	22	7.1E-5	193	0.122	0.321	1.7	8.24	2.0	0.4257	1.4	0.677	0.1403	1.50	2287	27	2231	26	-3.0
9711-53.1	61	66	1.13	24	5.4E-5	98	0.094	0.329	1.5	8.93	1.5	0.4538	1.3	0.877	0.1427	0.74	2412	27	2260	13	-8.1
9711-138.1	46	46	1.05	16	1.0E-4	39	0.175	0.291	2.2	8.02	1.7	0.4050	1.4	0.851	0.1436	0.87	2192	26	2271	15	4.1
9711-16.2	83	82	1.01	27	7.6E-5	110	0.132	0.278	2.0	7.59	1.7	0.3820	1.4	0.795	0.1442	1.03	2086	24	2278	18	9.9
9711-74.1	265	302	1.17	98	1.5E-5	28	0.025	0.344	0.8	8.60	1.3	0.4295	1.3	0.975	0.1452	0.29	2303	25	2291	5	-0.7
9711-16.1	59	59	1.03	21	5.2E-5	36	0.089	0.292	2.7	8.70	1.5	0.4260	1.4	0.898	0.1480	0.67	2288	26	2323	11	1.8
9711-95.1	80	79	1.01	29	4.2E-5	34	0.072	0.295	1.6	8.55	1.5	0.4168	1.4	0.924	0.1488	0.56	2246	26	2332	10	4.4
9711-30.1	101	119	1.22	38	2.9E-5	36	0.050	0.353	1.3	9.02	1.4	0.4376	1.3	0.931	0.1494	0.52	2340	26	2339	9	0.0
9711-9.1	95	112	1.23	36	6.7E-5	31	0.116	0.354	1.3	9.29	1.4	0.4469	1.3	0.927	0.1507	0.53	2381	26	2354	9	-1.4
9711-53.2	83	96	1.19	29	6.2E-5	30	0.107	0.341	1.7	8.51	1.5	0.4047	1.3	0.897	0.1524	0.66	2191	25	2374	11	9.1
9711-17.1	68	65	1.00	27	4.3E-5	31	0.075	0.296	1.6	10.02	1.6	0.4629	1.5	0.938	0.1571	0.57	2452	31	2424	10	-1.4

Notes (*see* Stern, 1997):

Spot name follows the convention x-y.z; where x = sample number, y = grain number, and z = spot number.

--- below detection

Corr Coeff = correlation coefficient

Uncertainties reported at 1σ and are calculated by using SQUID 2.23.08.10.21, rev. 21 Oct 2008.

$f206^{204}$ refers to mole per cent of total ^{206}Pb that is due to common Pb, calculated using the ^{204}Pb method; common Pb composition used is the surface blank (4/6: 0.05770; 7/6: 0.89500; 8/6: 2.13840).

* Refers to radiogenic Pb (corrected for common Pb).

Discordance relative to origin = 100 * ((207/206 age -206/238 age)/($^{207}Pb/^{206}Pb$ age)).

Calibration standard 6266; U = 910 ppm; age = 559 Ma; $^{206}Pb/^{238}U$ = 0.09059.

Error in $^{206}Pb/^{238}U$ calibration 1.2% (included).

Standard error in standard calibration was 0.29% (not included in above errors but required when comparing data from different mounts).

Analytical details: mount IP519, 25 μm spot size, primary beam intensity 14nA O_2^-, 6 scans.

Table 2. Uranium-lead TIMS analytical data.

	08CYA-C179A-02 NAD83, zone 17, 7229632N 362716E						Isotopic ratios[6]								Ages (Ma)[8]						
Fract.[1]	Description[2]	Wt. (ug)	U (ppm)	Pb[3] (ppm)	$^{206}Pb/^{204}Pb$[4]	Pb[5] (pg)	$^{208}Pb/^{206}Pb$	$^{207}Pb/^{235}U$	±1SE Abs	$^{206}Pb/^{238}U$	±1SE Abs	Corr.[7] Coeff.	$^{207}Pb/^{206}Pb$	±1SE Abs	$^{206}Pb/^{238}U$	±2SE	$^{207}Pb/^{235}U$	±2SE	$^{207}Pb/^{206}Pb$	±2SE	% Disc
Z1A (1)	Pk, Clr, rln, Eu, El, Dia	9	187	92	9378	5	0.09	10.377	0.012	0.4575	0.0004	0.944	0.16450	0.00007	2428.5	3.5	2469.0	2.1	2502.5	1.4	3.6
Z1B (1)	Pk, Clr, rln, Eu, El, Dia	9	211	92	20289	2	0.07	8.560	0.010	0.4135	0.0004	0.946	0.15015	0.00006	2230.9	3.3	2292.4	2.0	2347.7	1.4	5.9
Z2A (1)	Pk, Clr, rln, Eu, El, Dia	13	246	97	42259	2	0.06	7.330	0.008	0.3839	0.0003	0.942	0.13848	0.00006	2094.5	3.2	2152.5	2.0	2208.3	1.4	6.0
Z2B (1)	Pk, Clr, rln, Eu, El, Dia	22	191	86	68071	2	0.08	9.110	0.010	0.4273	0.0004	0.945	0.15462	0.00006	2293.7	3.4	2349.1	2.1	2397.7	1.4	5.2
Z3A (1)	Co, Clr, rln, Eu, Eq, Dia	12	203	92	41373	2	0.09	8.983	0.010	0.4236	0.0004	0.947	0.15379	0.00006	2277.0	3.5	2336.3	2.1	2388.5	1.4	5.5
Z3B (1)	Co, Clr, rln, Eu, Eq, Dia	14	123	62	28832	2	0.11	10.594	0.012	0.4628	0.0004	0.941	0.16601	0.00007	2452.0	3.7	2488.2	2.1	2517.9	1.4	3.2

Notes:
[1]Z = zircon fraction; Number in brackets refers to the number of grains in the analysis.
[2]Zircon descriptions: Co = colorless, Pk = pink, Clr = clear, rln = rare inclusions, Eu = euhedral, El = elongate, Eq = equant, Dia = diamagnetic.
[3]Radiogenic Pb.
[4]Measured ratio, corrected for spike and fractionation.
[5]Total common Pb in analysis corrected for fractionation and spike.
[6]Corrected for blank Pb and U and common Pb, errors quoted are 1σ absolute; procedural blank values for this study are 0.1 pg U and 1 pg Pb.
Pb blank isotopic composition is based on the analysis of procedural blanks; corrections for common Pb were made using Stacey and Kramers (1975) compositions.
[7]Correlation coefficient
[8]Corrected for blank and common Pb, errors quoted are 2σ in Ma.
The error on the calibration of the GSC ^{205}Pb-^{233}U-^{235}U spike utilized in this study is 0.22% (2σ).

granoblastic texture that overprints and partially obscures gneissic layering. Across the exposure, the anorthosite unit is cut by several 3–5 m wide pale pink-weathering monzogranite pegmatite dykes at a high angle to gneissosity (Fig. 2b).

Zircon grains are diverse in appearance, with some clear and colourless, whereas others have an orange stain. Many grains are characterized by distinct cores and rims, whereas others are composed of a single phase of zircon. Single-component zircon may exhibit oscillatory zoning, but may also be unzoned (Fig. 2d, e). Core-rim relationships are visible in plane light (Fig. 2c), as well as in BSE images (e.g. Fig. 2f, g, h). Both zoned and unzoned zircon may be present as cores. Two chemically distinct rims have been indentified: 1) unzoned low-U (dark BSE) rims with Th abundances less than 0.3 ppm (Fig. 2h), and 2) unzoned high-U (bright zones in BSE *see* Fig. 2f, g), low Th/U (0.03–0.08) rims. Zircon grains with similar chemistry to both types of rims are also present as single-component grains.

Archean ages ranging from 3.0 Ga to 2.7 Ga are documented from cores and oscillatory-zoned zircon (Table 1, Fig. 2i). Replicate analyses on individual grains are not reproducible and most of these analyses are between 5% and 30% discordant. The scatter and relatively large amounts of discordance in the Archean data set complicate the interpretation of these results. The data define a discordant array along a discordia between the age of the oldest analyses and Paleoproterozoic ages recorded by zircon rims. This trend is consistent with a Paleoproterozoic overprint of a single population of zircon the age of which is constrained by the oldest, most concordant result. Based on these observations, the authors consider that the best estimate of the crystallization age of the anorthosite is 3007 ± 14 Ma (grain 84, 2σ error).

Single-phase grains or zircon rims with low U and negligible Th are common, however, only five zircons with sufficient U (20–200 ppm U) to yield a result with useful precision were analyzed. These yield a weighted mean $^{207}Pb/^{206}Pb$ age of 1886 ± 17 Ma. The high-U overgrowths range in age from 1850 Ma to 1880 Ma, with a dominant mode of 1.865 Ga, but do not yield a single statistical population. Both of these zircon populations have low, to extremely low, Th/U ratios consistent with a metamorphic origin.

The low-U character of the ca. 3.0 Ga population recovered from 08CYA-J148a is consistent with crystallization from an anorthositic magma, whereas the low-U low-Th grains and rims are chemically consistent with a metamorphic origin, independently established in this region at 1.88 Ga and 1.86 Ga (Berman et al., 2011). The present authors propose infiltration of a fluid derived from cross-cutting pegmatite dykes, as evidenced by presence of trace apatite in anorthosite proximal to pegmatite, as the cause of ca. 1.865 Ga high-U zircon growth.

Table 3. SHRIMP trace-element results from selected zircon grains from sample 08CYA-M243.

Spot name	Ti	Y	Ba	La	Ce	Pr	Nd	Sm	Eu	Gd	Dy	Ho	Er	Tb	Lu	Ta	Tm	Yb	Hf	Th	U	Ce*	Eu*	Age (Ma)
9711-3.1	12	538	0.029	0.006	5.5	0.078	0.97	2.03	0.45	10.9	46	17.1	80	3.5	30	0.8	17.4	174	10337	237	160	62.6	0.293	2047
9711-3.2	13	538	0.041	0.131	6.0	0.129	1.36	2.38	0.52	12.2	50	18.5	83	4.1	33	0.6	19.0	178	10315	250	160	11.2	0.295	2067
9711-9.1	27	374	0.032	0.007	4.3	0.074	0.65	1.32	0.26	7.2	32	12.2	57	2.5	21	0.5	12.6	116	7912	107	89	44.1	0.257	2354
9711-17.1	23	166	0.026	0.006	3.4	0.060	0.39	0.64	0.14	3.3	15	5.4	26	1.1	10	0.5	5.9	56	8500	58	60	45.2	0.288	2424
9711-29.1	12	248	0.025	0.005	4.5	0.049	0.39	0.67	0.18	4.1	20	7.8	38	1.4	17	0.5	8.9	92	9419	141	125	70.3	0.330	2021
9711-29.2	9	252	0.030	0.005	4.9	0.027	0.28	0.61	0.15	4.1	20	8.0	40	1.4	17	0.7	9.0	94	9874	147	140	100.8	0.290	2026
9711-33.1	12	231	0.035	0.029	4.8	0.088	0.94	0.99	0.19	4.4	20	7.5	36	1.5	14	0.5	8.4	79	7323	78	77	23.1	0.271	2040
9711-33.2	10	212	0.024	0.019	4.4	0.054	0.52	0.81	0.17	3.9	18	6.8	32	1.3	13	0.4	7.2	72	7525	77	70	33.0	0.283	2049
9711-53.1	14	222	0.033	0.012	4.0	0.047	0.51	0.96	0.26	4.8	20	7.2	34	1.5	14	0.5	7.4	76	7872	66	60	39.9	0.372	2260
9711-53.2	17	246	0.023	0.007	3.7	0.032	0.55	0.95	0.27	5.1	21	7.9	38	1.6	16	0.6	8.4	83	8826	85	72	61.3	0.379	2374
9711-72.1	10	332	0.021	0.005	4.7	0.037	0.40	0.85	0.21	5.2	26	10.5	52	1.9	22	0.7	11.4	123	10820	152	138	86.6	0.300	2045
9711-72.2	14	299	0.022	0.005	4.3	0.034	0.41	0.84	0.20	5.3	25	9.6	47	1.8	20	0.6	10.9	109	10607	128	112	83.9	0.295	2078
9711-74.1	12	639	0.045	0.007	6.5	0.052	0.67	1.67	0.45	10.8	53	20.1	99	3.7	41	0.7	21.9	219	7447	306	248	82.9	0.320	2291
9711-74.2	17	148	0.031	0.013	3.5	0.044	0.31	0.47	0.14	2.5	12	4.7	24	0.9	11	0.7	5.6	59	9814	60	71	35.7	0.401	2041
9711-78.1	13	355	0.037	0.023	4.5	0.057	0.57	1.09	0.30	6.4	30	11.4	56	2.1	23	0.6	12.5	129	10014	134	105	30.0	0.346	2072
9711-78.2	15	268	0.025	0.004	3.6	0.031	0.38	0.80	0.21	4.7	22	8.6	42	1.6	17	0.6	9.4	94	9195	92	77	79.5	0.329	2075
9711-91.1	10	252	0.040	0.013	5.2	0.043	0.41	0.72	0.19	4.1	21	7.8	40	1.4	18	0.4	9.6	99	8396	140	136	53.8	0.335	2017
9711-91.2	8	261	0.020	0.004	4.9	0.037	0.28	0.54	0.16	3.6	19	7.9	41	1.3	20	0.5	9.6	105	9048	136	154	101.3	0.349	2061
9711-95.1	21	269	0.026	0.003	3.9	0.046	0.41	0.85	0.17	5.0	23	8.7	41	1.7	15	0.5	8.8	88	7830	82	80	78.1	0.251	2332
9711-95.2	21	214	0.026	0.005	3.6	0.026	0.33	0.66	0.14	3.8	18	6.9	33	1.3	12	0.4	7.0	71	7297	76	75	80.3	0.268	2154
9711-96.1	7	373	0.030	0.007	6.3	0.045	0.50	0.97	0.22	6.0	30	11.7	58	2.0	25	0.6	12.9	134	11053	143	149	87.0	0.275	2025
9711-96.2	6	277	0.040	0.006	4.1	0.033	0.38	0.81	0.19	4.7	23	8.9	43	1.6	18	0.5	9.9	98	9799	102	103	68.5	0.297	2004

Notes:
Grain and analysis numbering keyed to identical numbering on U-Pb Table 1.
Ce* = Ce anomaly ($Ce_{chondrite\ norm}/SQRT(La_{chondrite\text{-}norm}*Pr_{chondrite\text{-}norm})$).
Eu* = Eu anomaly ($Eu_{chondrite\ norm}/SQRT(Sm_{chondrite\text{-}norm}*Gd_{chondrite\text{-}norm})$).
Detection limit is about 3 ppb.
Age information is taken directly from Table 1.

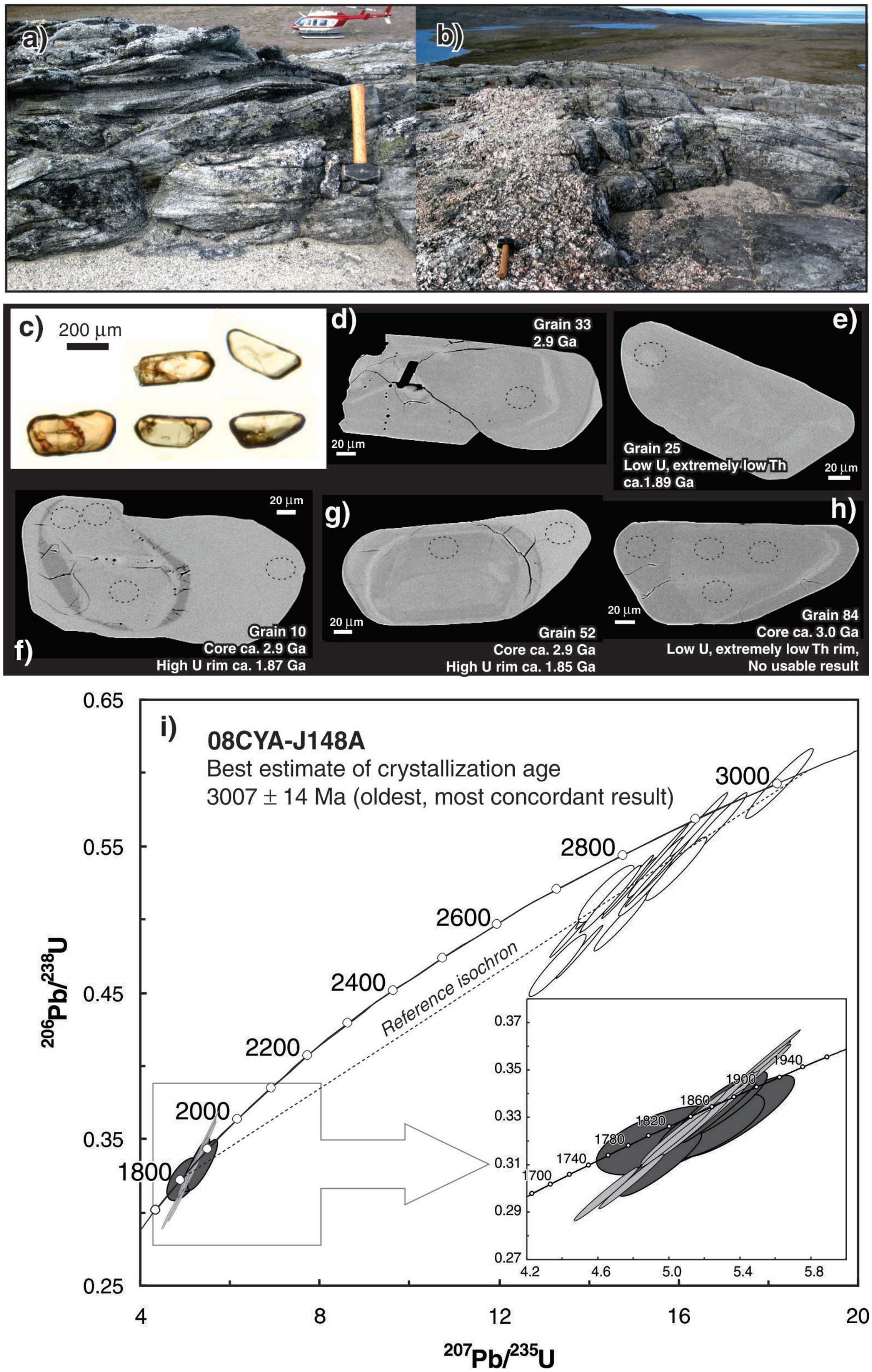

Figure 2. a) Strongly recrystallized Nalojoaq anorthosite 08CYA-J148; note unconsolidated plagioclase grit-weathered material. Photograph by M. Sanborn-Barrie. 2013-011. **b)** Overview of exposure showing a crosscutting pegmatite dyke. Photograph by M. Sanborn-Barrie. 2013-013. **c)** Plane-light image of zircon selected for SHRIMP U-Pb analysis. **d), e), f), g), h)** Corresponding back-scattered electron images of zircon grains shown in Figure 2**c**. *See* text for description. **i)** Concordia diagram of zircon SHRIMP analyses. Interpreted igneous zircon shown by white ellipses, low-U zircon grains and rims shown by dark grey ellipses, high-U rims and grains shown by light grey ellipses. Error ellipses are 2σ. Dashed line represents a free regression through the data. Inset: detail of Paleoproterozoic zircon results. *See* text for discussion.

Sample 08CYA-C177A (z9708) amphibole-biotite-orthopyroxene tonalite

A significant component of Southampton Island's basement complex (Fig. 1b) is composed of a granulite-grade (orthopyroxene-bearing) gneissic suite that also occurs as enclaves within regionally extensive biotite-hornblende-granodiorite. Two geographically widespread samples were collected in order to evaluate the age of this suite. A sample of orthopyroxene tonalite was collected from the north (C177; Fig. 1b), whereas an orthopyroxene-biotite quartz diorite (C106a; Fig. 1b, results given below) was collected from the south, near the hamlet of Coral Harbour.

Sample C177 was taken from a 20 m by 10 m tonalitic enclave within biotite-hornblende-granodiorite. Internal to the tonalite (not shown) are elongate melanocratic gabbroic inclusions that may be tightly folded. Collectively, these lithologies are cut by foliation-parallel monzogranite veins (Fig. 3a). Zircon grains extracted from the sample are predominantly equant to stubby prisms with resorbed and/or rounded facets with a small number of more elongate prismatic grains. Faint oscillatory zoning is observed in many zircon grains, commonly as cores surrounded by unzoned rims (Fig. 3b, grain 3). In other cases, there is a discordant, but diffuse contact between oscillatory-zoned zircon and patchy, unzoned zircon suggestive of partial recrystallization (Fig. 3b, grain 63). Twenty-three zircon grains analyzed yielded dates ranging from 2774 Ma to 1972 Ma, forming an array with a cluster of concordant ages at 2770 ± 6 Ma (weighted mean $^{207}Pb/^{206}Pb$ age, n = 6, MSWD = 2.4), and a Paleoproterozoic lower intercept (Table 1, Fig. 3b). Given the evidence for partial recrystallization, the zonation patterns in the BSE images, and the evidence for Trans-Hudson Orogen related metamorphism of this region (Berman et al., 2011; Rayner et al., 2011), these younger ages are suspected to reflect variable degrees of Pb loss. The weighted mean $^{207}Pb/^{206}Pb$ age of 2770 ± 6 Ma for the six oldest grains is interpreted as the crystallization age of the orthopyroxene-bearing tonalite.

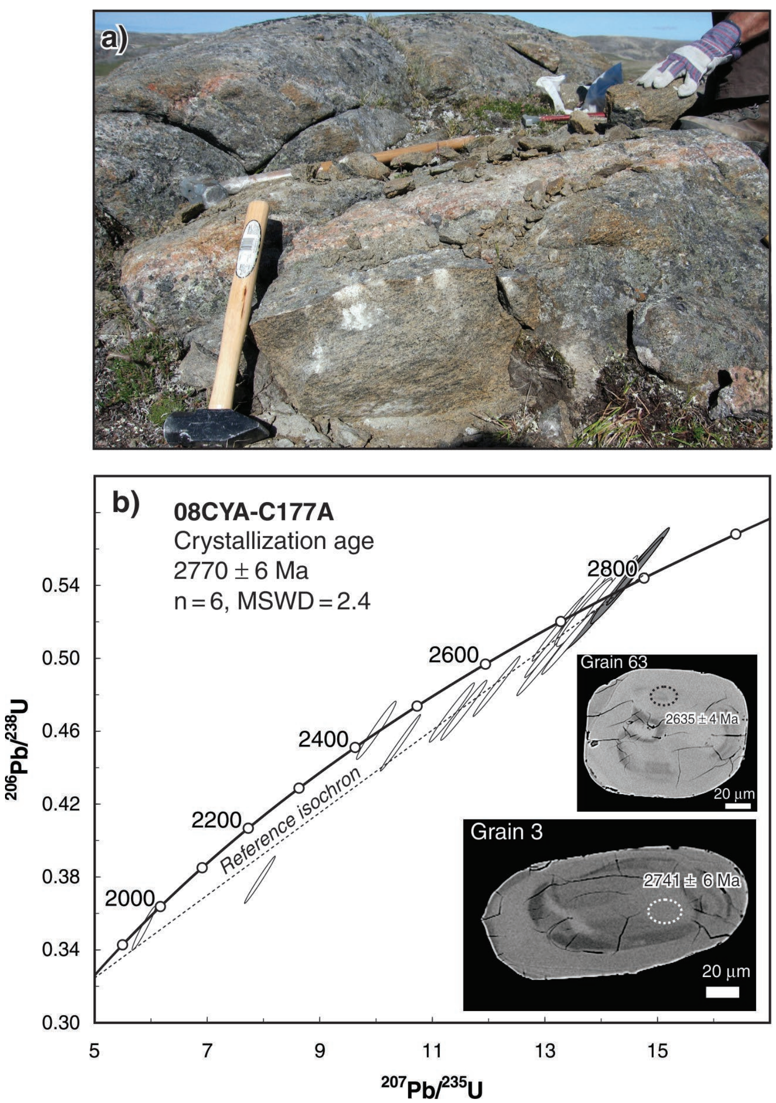

Figure 3. a) Greasy-green–weathering orthopyroxene-bearing tonalite from which sample 08CYA-C177 was collected. Hammer is approximately 27.5 cm in length. Photograph by J. Chakungal. 2013-010. **b)** Concordia diagram for zircon SHRIMP analyses for 08CYA-C177. Error ellipses are 2σ. The crystallization age is calculated with the five oldest analyses highlighted in grey. Inset: backscatter images (spot error reported at 1σ) representative of types of overgrowths and/or recrystallization textures observed in the zircon grains.

Sample 08CYA-C106a (z9707) orthopyroxene-biotite quartz diorite

Sample C106a is strongly foliated, medium-grained orthopyroxene-bearing quartz diorite containing abundant dioritic-noritic xenoliths, within which garnet porphyroblasts mantled by plagioclase occur locally. The greasy-green fresh surfaces are interpreted to reflect high-temperature modification of feldspar, and together with orthopyroxene±garnet assemblages support granulite-facies metamorphism of these rocks, prior to intrusion of pink-weathering biotite alkali-feldspar monzogranite (Fig. 4a).

Zircon grains are mostly 200 µm long or less, rounded to subhedral prisms characterized by oscillatory zoning. Many grains are distinguished by rims low in U relative to their distinct cores (i.e. grain 19 Fig. 4b), with high-U rims only rarely observed. Thirty-one analyses were conducted on 27 separate zircon grains encompassing the full range of morphological characteristics. The results range in age from 3.2 Ga to 1.8 Ga (Table 1, Fig. 4b). The oldest results, between 3185 Ma and 2820 Ma, are derived largely from cores and are interpreted as inherited based upon the spread in these older ages. The majority of the $^{207}Pb/^{206}Pb$ results range between 2763 Ma and 2622 Ma, with a small cluster of analyses at the upper end of this range. The weighted mean of the seven oldest zircon grains from this population, which consist of mainly single-phase zircon, yield an age of 2757 ± 5 Ma (MSWD = 1.8). The ages of low-U rims (ca. 2.73 Ga to 2.62 Ga) overlap those of the cores and single phase zircons, however, the low-U rims tend to cluster at slightly younger ages (ca. 2.72 Ga). Given the complex nature if these results, the authors are unable to demonstrate that the low-U overgrowths with ages that cluster at ca. 2.72 Ga are distinct from the 2757 ± 5 Ma population and consider this older age as the best estimate for the time of crystallization. Analyses of two high-U rims yielded Paleoproterozoic ages of 1819 ± 4 Ma and 1968 ± 7 Ma: the former (4% discordant) is attributed to fluid related to crosscutting monzogranite and the latter (18% discordant) likely due to overlap of the analytical pit on a thin, high-U overgrowth with an Archean core.

Sample 08CYA-C179a (z9709) deformed amphibole-biotite monzogranite

A sample of homogeneous, strongly deformed biotite-magnetite monzogranite was collected from near Cape Arvinguaq in the northeast quadrant of the exposed basement (Fig. 1b). Here, highly tectonized, feldspar porphyroclastic straight gneiss displays a very strongly developed L>S fabric defined by ribboned quartz and continuous seams of biotite (Fig. 5a) oriented 240/68°NW, and a strong, shallow, west-plunging mineral lineation. This locality coincides with a positive aeromagnetic anomaly with a strike length of 35 km and breadth of 8 km, which reflects a predominance of variably strained, magnetite-bearing granitic rocks. This sample was collected to constrain the magmatic age of a regionally extensive unit and provide a maximum age of localized high strain, established elsewhere on the basis of overprinting structural fabric relationships as regional D_2.

Zircon grains recovered include high-quality, clear, pale pink elongate prisms as well as high-quality, clear, colourless equant grains. Due to the high quality of the zircon grains and apparently simple morphologies, this sample was analyzed using the ID-TIMS technique. Core-overgrowth relationships, observed in some cases, were avoided in the grains selected for analysis (Fig. 5b, inset i). Six single-grain fractions of elongate and equant zircons (Table 2) were analyzed via ID-TIMS after being chemically abraded for 6 hours at 180°C according to a method modified from that of Mattinson (2005). Six single-grain fractions are between 3% to 6% discordant and are strongly colinear (Fig. 5b). A regression through all six fractions (MSWD = 1.6) yields an upper intercept age of 2618 ± 4 Ma and a lower intercept of 1844 ± 7 Ma. Given the strain state of the monzogranite, as well as tectonometamorphic constraints from in situ U-Pb monazite dating that establish regional D_2 deformation and associated metamorphism (M_4) at 1.86–1.84 Ga (Berman et al., 2011), the present authors interpret the upper intercept age of 2618 ± 4 Ma to represent the crystallization age, and the lower intercept age of ca. 1.84 Ga to reflect penetrative Paleoproterozoic D_2M_4 tectonometamorphism. Subsequent SEM imaging (*see* Fig. 5b, inset ii) of zircon grains from this sample revealed the presence of thin, unzoned high-U overgrowths as well as diffuse patchy zoning, not visible in plane light, both of which are texturally consistent with a Paleoproterozoic metamorphic overprint.

Sample 08CYA-M243a (z9711) gabbroic anorthosite

Gabbro and gabbroic anorthosite occupy the southwest part of the exposed basement complex and occur as an isolated inlier 80 km southwest of Coral Harbour (M98; Fig. 1b). In general, this mafic unit comprises weakly to strongly foliated gabbro, leucogabbro, and gabbroic anorthosite composed of 50–20% hornblende-biotite±clinopyroxene±garnet. In least-strained exposures, mafic phases occur as 3–8 mm clots set in a fine-grained recrystallized groundmass of plagioclase (Fig. 6a, inset). A more evolved leucogabbro with 2% modal quartz (08CYA-M243; Fig. 1b) was selected for U-Pb dating to increase the likelihood of zircon being present as an accessory phase. The strain state of this gabbroic body is variable with clear evidence for two generations of fabrics. Local recognition of both generations of tectonic fabrics in this mafic pluton (Fig. 6a) allows that its crystallization age is a maximum age of regional D_1 and D_2 deformation in this part of the basement complex.

Zircon grains are clear, colourless, anhedral fragments or equant prisms (Fig. 6b, inset). Anhedral fragments yield a weighted mean $^{207}Pb/^{206}Pb$ age of 2058 ± 4 Ma, which is interpreted as the crystallization age (Table 1, Fig. 6b).

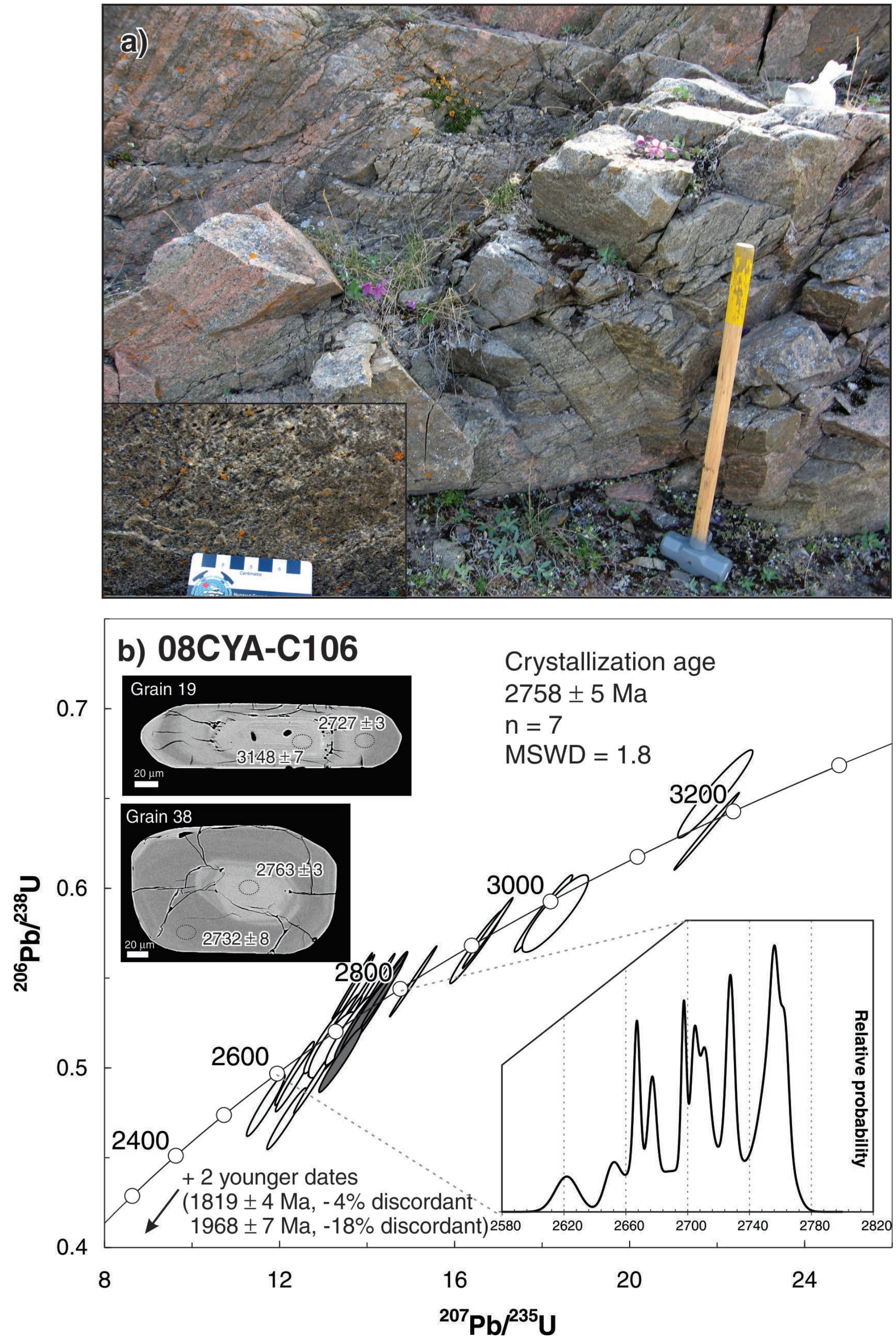

Figure 4. a) Greasy-green–weathering orthopyroxene-bearing quartz diorite from which sample 08CYA-C106 was collected. Hammer is approximately 80 cm in length. Photograph by J. Chakungal. 2013-014. Inset: Photograph by J. Chakungal. 2013-009. **b)** Concordia diagram for zircon SHRIMP analyses. Error ellipses are 2σ. The crystallization age is calculated using the seven analyses highlighted in grey. Two discordant Paleoproterozoic results are not shown, but their ages and error are reported at the 1σ uncertainty level. *See* text for discussion. Inset: backscatter images (spot error reported at 1σ) representative of the textures observed in the zircon grains. Probability density diagram of the interpreted igneous zircons (2780 Ma to 2620 Ma).

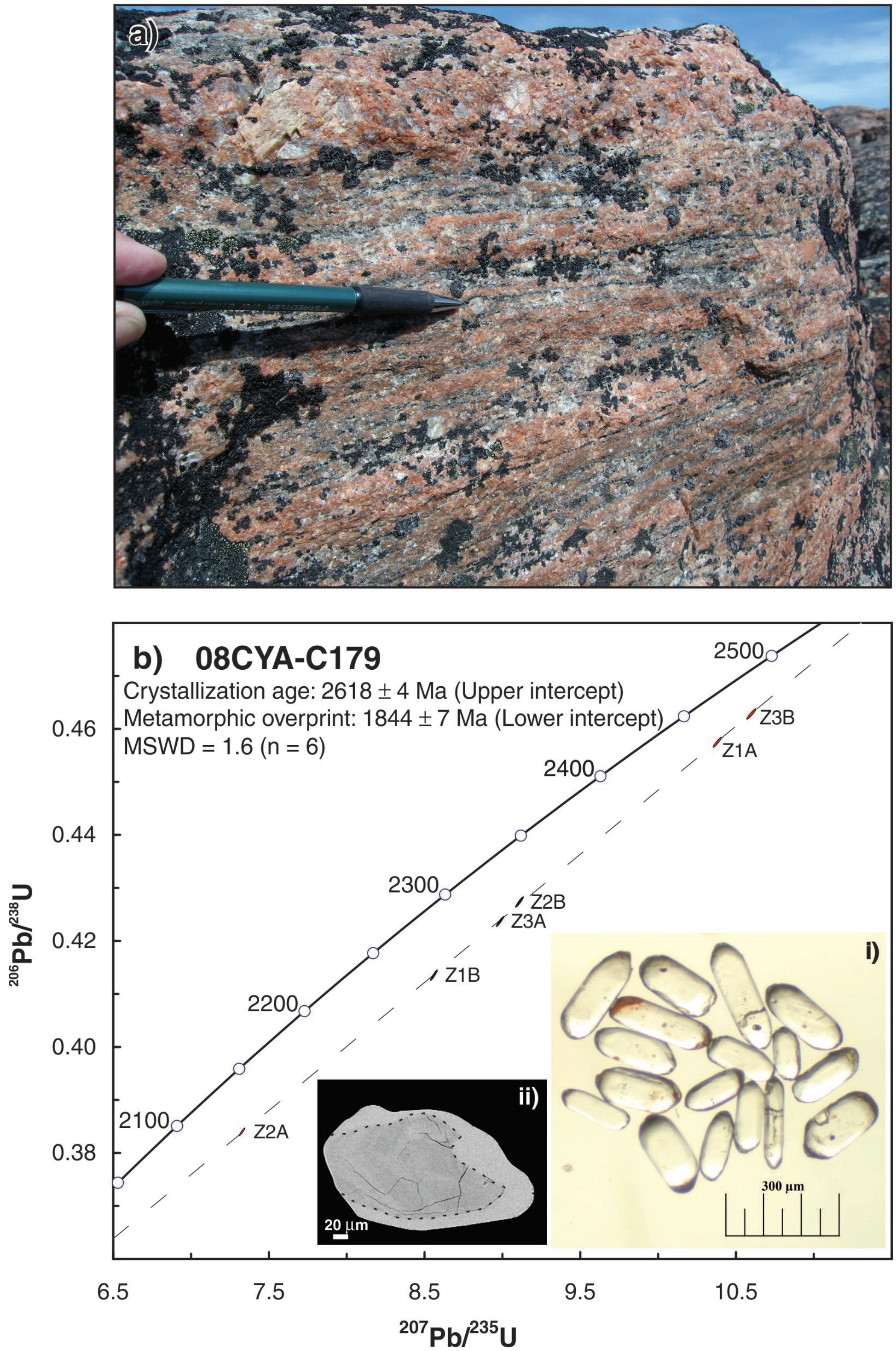

Figure 5. a) Strongly deformed to mylonitic monzogranite from locality 08CYA-C179. Photograph by M. Sanborn-Barrie. 2013-008. **b)** Concordia diagram of zircon TIMS analyses. Error ellipses are 2σ. Inset i: plane-light image of zircon where core and/or overgrowth textures are not evident selected for TIMS analysis. Inset ii: back-scattered electron image of representative zircon that displays subtle core-overgrowth relationship.

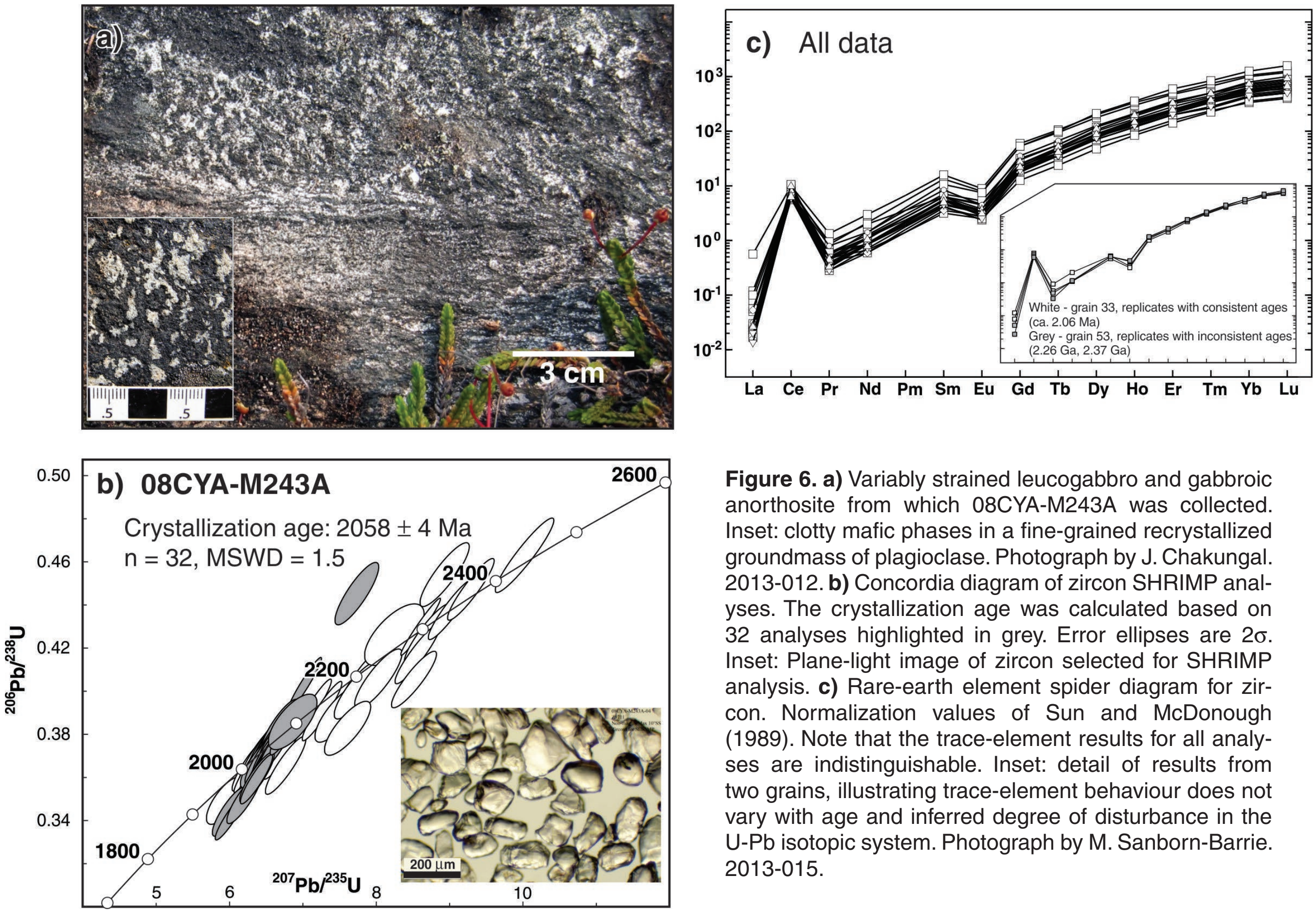

Figure 6. a) Variably strained leucogabbro and gabbroic anorthosite from which 08CYA-M243A was collected. Inset: clotty mafic phases in a fine-grained recrystallized groundmass of plagioclase. Photograph by J. Chakungal. 2013-012. **b)** Concordia diagram of zircon SHRIMP analyses. The crystallization age was calculated based on 32 analyses highlighted in grey. Error ellipses are 2σ. Inset: Plane-light image of zircon selected for SHRIMP analysis. **c)** Rare-earth element spider diagram for zircon. Normalization values of Sun and McDonough (1989). Note that the trace-element results for all analyses are indistinguishable. Inset: detail of results from two grains, illustrating trace-element behaviour does not vary with age and inferred degree of disturbance in the U-Pb isotopic system. Photograph by M. Sanborn-Barrie. 2013-015.

Some fragments and equant prisms plot along concordia as a broadly linear array with $^{207}Pb/^{206}Pb$ ages up to 2424 Ma; however, morphology, zoning, and U-Th composition do not correlate with these older ages. The array of older results may be indicative of partial recrystallization with accompanying Pb loss from an inherited population. Trace element analyses were subsequently carried out to aid in the recognition of any cryptic, older phases. All zircon grains, regardless of age, have overlapping trace-element compositions exhibiting a pattern diagnostic of magmatic zircon, with positive Ce anomalies, negative Eu anomalies, and strong HREE enrichment (Fig. 6c; Hoskin and Schaltegger, 2003). Assuming that the inherited grains belong to a single population, consistent with their homogeneous appearance and chemical characteristics, the U-Pb systematics of which have been affected by the emplacement of the leucogabbro, the $^{207}Pb/^{206}Pb$ age of the oldest inherited zircon (2424 Ma) would represent the minimum age of that population.

DISCUSSION AND CONCLUSIONS

Rayner et al. (2011) presented the first U-Pb age determinations from Southampton Island that documented local existence of Archean granitoid rocks and underscored the importance of Paleoproterozoic magmatism and tectonometamorphic reworking in this region. The additional data presented here further establishes the Archean ancestry of Precambrian rocks exposed across Southampton Island, revealing that they are more extensive and older than recognized by the initial dating program. The new U-Pb data support field observations that mafic plutonic rocks represent some of the oldest lithological components exposed on Southampton Island (Sanborn-Barrie et al., 2008). Mafic-ultramafic-anorthositic rocks commonly occur as deformed enclaves contained within the orthopyroxone-bearing tonalite-granodiorite-granite gneiss complex, previously dated at ca. 2.7 Ga (Rayner et al., 2011) and here established to include significant ca. 2.77–2.76 Ga phases. Anorthosite sample 08CYA-J148A yielded a direct age constraint on the ancient mafic plutonic phase, with an interpreted crystallization age of 3.0 Ga. This agrees with the reinterpretation of U-Pb data from a sample of gabbroic anorthosite (M38B) from a layered mafic-ultramafic intrusion located 150 km to the northwest (Fig. 1b). Previously, a significant population of ca. 3 Ga zircon was considered to be xenocrystic in origin (Rayner et al., 2011); however, integration of zircon morphology, U-Pb data and recently acquired rare-earth–element data for different age populations of zircon separates (Rayner et al., 2012) collectively presented a strong case for ca. 3 Ga crystallization with a 1870 ± 10 Ma metamorphic overprint, the latter consistent with the timing of metamorphism reported by Berman et al. (2011). Both dated anorthositic units comprise relatively large bodies (100 m to kilometre scale) that display high (J148) to moderate (M38) strain and pervasive crystallization. While these samples document an episode of mafic magmatism at ca. 3 Ga, one cannot rule out additional mafic plutonic events to account for other mafic plutonic enclaves within the 2.77–2.76 Ga gneissic suite.

Two of the samples analyzed in this study contribute further insight into the Neoarchean magmatic evolution of Southampton Island. Orthopyroxene-bearing tonalite (08CYA-C177) yields a crystallization age of 2772 ± 3 Ma, which is consistent with this unit occurring as enclaves within regionally extensive granodiorite, the latter unit dated at 2692 ± 6 Ma (Rayner et al., 2011) at a locality 8 km to the west (M62, Fig. 1b). Notably, older inherited zircon was not recovered from this sample, as might be expected given its crustal residence age of 3.3 Ga (Whalen et al., 2011). Orthopyroxene-bearing quartz diorite (08CYA-C106) yields a crystallization age of 2758 ± 5 Ma. This sample has an identical Nd model age as the orthopyroxene-bearing tonalite, but in this sample, an inherited component at 3.2 Ga, 3.0 Ga, and 2.9 Ga is documented by the zircon data. These results establish that regionally extensive granulite facies plutonic rocks are Neoarchean in age, and that the ca. 1.93 Ga age reported for sample B99 (Fig. 1b) in Rayner et al. (2011) is not representative of basement on Southampton Island. Uranium-lead basement crystallization ages between 2.77–2.75 Ga with Nd model ages of 3.6 Ga to 3.0 Ga (Whalen et al., 2011) support correlation of Southampton Island with the northeast Rae craton.

The crystallization age of 2618 ± 4 Ma for mylonitic biotite-magnetite monzogranite (08CYA-C179) suggests that a suite of ca. 2.6 Ga granitic rocks that transect the Rae craton to the northwest (Hinchey et al., 2011) and to the north (N. Wodicka, unpub. data, 2011) are represented on Southampton Island, further strengthening the island's affinity with Rae crust. With an Sm-Nd model age of 2.88 Ga, one of the youngest derived from samples across the island (Whalen et al., 2011), this 2.61 Ga phase displays little evidence in its isotopic systematics for involvement of older inherited material.

In the southwest, variably strained gabbroic anorthosite (08CYA-M243A) yielded an age of 2058 ± 4 Ma. Rocks of this age are rare in Laurentia, but where observed, they are associated with rift-related rocks on Cape Smith (e.g. Modeland et al., 2003), the Nain plutonic suite (Hamilton et al., 1998), and as dykes transecting the Hearne (Pehrsson et al., 1993) and Superior (Buchan et al., 1996) cratons. Accordingly, this gabbroic unit may reflect ca. 2.0 Ga extension, possibly related to sustained extension during opening of the Manikewan ocean (Stauffer, 1984; Halls and Heaman, 2000). Its 2.058 Ga age provides a maximum age of the two deformation events (Fig. 6a) that affected this region, consistent with the interpretation that penetrative D_1 and D_2 are 1880 Ma and 1860–1840 Ma, respectively (Berman et al., 2012).

The data presented herein not only expand insight into the Archean magmatic evolution of Southampton Island, but they further document the effects of Paleoproterozoic tectonometamorphism (Rayner et al., 2011; Berman et al., 2011, 2012). For instance, considerable Paleoproterozoic Pb loss is shown by zircon grains from samples 08CYA-C177 and 08CYA-C106, consistent with profound magmatic and tectonometamorphic reworking across the island at 1.88–1.82 Ga. Sample 08CYA-C179 yields an ID-TIMS lower intercept age of 1844 ± 7 Ma, the result of incorporating Paleoproterozoic zircon rims during dilution. Zircon grains from anorthosite 08CYA-J148 possess low Th rims dated at 1886 ± 17 Ma, and high-U rims at ca. 1.865 Ga. Zircon grains with similar compositions and Paleoproterozoic ages have been documented from complex orthogneiss outcrops on Mill and Salisbury islands (Fig. 1a) located approximately 250 km to the east in Hudson Strait (Rayner et al., 2008). These Paleoproterozoic ages are consistent with long-lasting, penetrative involvement in the Trans-Hudson collision between the Rae and Superior cratons.

ACKNOWLEDGMENTS

The Southampton Island Integrated Geoscience project was funded by the Canada-Nunavut Geoscience Office through a Strategic Investments in Northern Economic Development (SINED) initiative and by the Geological Survey of Canada's Northern Mineral Resources and Development (NMRD) program. Logistical support was co-ordinated by Natural Resources Canada's Polar Continental Shelf Program. Mapping and sample collection by J. Whalen and D. James contributed to the authors' understanding of Southampton Island's plutonic rock record. The authors thank P. Hunt, T. Pestaj, J. Peressini, L. Cataldo, and C. Lafontaine for their expert assistance in acquiring SEM, SHRIMP, and ID-TIMS results, respectively. A constructive review of this paper was provided by B. Davis.

REFERENCES

Berman, R.G., Rayner, N., Sanborn-Barrie, M., and Chakungal, J., 2011. New constraints on the tectonothermal history of Southampton Island, Nunavut, provided by *in situ* SHRIMP geochronology and thermobarometry; Geological Survey of Canada, Current Research 2011-6, 14 p. doi:10.4095/287287

Berman, R.G., Sanborn-Barrie, M., Rayner, N., and Whalen, J., 2012. The tectonometamorphic evolution of Southampton Island, Nunavut: insight from petrological modeling and *in situ* SHRIMP geochronology of multiple episodes of monazite growth; Precambrian Research. doi:10.1016/j.precamres.2012.08.011

Buchan, K.L., Halls, H.C., and Mortensen, J.K., 1996. Paleomagnetism, U-Pb geochronology of Marathon dykes, Superior Province, and comparison with the Fort Frances swarm; Canadian Journal of Earth Sciences, v. 33, p. 1583–1595. doi:10.1139/e96-120

Chakungal, J., Sanborn-Barrie, M., and James, D., 2007. Southampton Island: an updated Geosciences database; *in* 35th Annual Yellowknife Geoscience Forum Abstracts, (comp.) S. Cairns and S. Falck; YKGSF Abstracts Volume 2007, November 20–22, 2007, Northwest Territories Geoscience Office, Yellowknife, Northwest Territories, p. 8–9.

Chakungal, J., Sanborn-Barrie, M., James, D., Rayner, N., Whalen, J., Craven, J., Spratt, J., Kosar, K., Ross, M., Zhang, S., and Coyle, M., 2008. Natural resource potential – yes or no? Southampton Island Integrated Project: a summary of 2007 & 2008 results and investigations; 36th Annual Yellowknife Geoscience Forum Abstracts, (comp.) V. Jackson and D. Irwin; YKGSF Abstracts Volume 2008, November 18–20, 2008, Northwest Territories Geoscience Office, Yellowknife, Northwest Territories, p. 66–67.

Halls, H.C. and Heaman, L.M., 2000. The paleomagnetic significance of new U-Pb age data from the Molson dyke swarm, Cauchon Lake area, Manitoba; Canadian Journal of Earth Sciences, v. 37, p. 957–966. doi:10.1139/e00-010

Hamilton, M.A., Ryan, A.B., Emslie, R.F., and Ermanovics, I.F., 1998. Identification of Paleoproterozoic anorthositic and monzonitic rocks in the vicinity of the Mesoproterozoic Nain Plutonic suite, Labrador; U-Pb evidence; Radiogenic Age and Isotopic Studies: Report 11, Current Research 1998-F, Geological Survey of Canada, p 23–40.

Hinchey, A., Davis, W.J., Ryan, J.J., and Nadeau, L., 2011. Neoarchean high-potassium granites of the Boothia mainland area, Rae domain, Churchill Province: U–Pb zircon and Sm–Nd whole rock isotopic constraints; Canadian Journal of Earth Sciences, v. 48, p. 247–279. doi:10.1139/E10-071

Hoskin, P.M.O. and Schaltegger, U., 2003. Composition of zircon and igneous and metamorphic petrogenesis; *in* Zircon, (ed.) J.M. Hanchar and P.W.O. Hoskin; Reviews in Mineralogy, v. 53, p. 27–62.

Ludwig, K.R., 2003. User's manual for Isoplot/Ex rev. 3.00: a geochronological toolkit for Microsoft Excel; Berkeley Geochronology Center, Special Publication 4, Berkeley, 70 p.

Mattinson, J.M., 2005. Zircon U-Pb chemical abrasion ("CA-TIMS") method: combined annealing and multi-step partial dissolution analysis for improved precision and accuracy of zircon ages; Chemical Geology, v. 220, p. 47–66. doi:10.1016/j.chemgeo.2005.03.011

Modeland, S., Francis, D., and Hynes, A., 2003. Enriched mantle components in Proterozoic continental-flood basalts of the Cape Smith foldbelt, northern Quebec; Lithos, v. 71, no. 1, p. 1–17. doi:10.1016/S0024-4937(03)00063-X

Parrish, R.R., Roddick, J.C., Loveridge, W.D., and Sullivan, R.W., 1987. Uranium-lead analytical techniques at the geochronology laboratory, Geological Survey of Canada; *in* Radiogenic Age and Isotopic Studies: Report 1, Geological Survey of Canada, Paper 87-2, p. 3–7.

Pehrsson, S.J., van Breemen, O., and Hanmer, S., 1993. Ages of diabase dyke intrusions, Great Slave Lake shear zone, Northwest Territories; *in* Radiogenic Age and Isotopic Studies: Report 7; Geological Survey of Canada, Paper 93-2, p. 23–28.

Rayner, N., Scott, D.J., Wodicka, N., and Kassam, A., 2008. New geochronological constraints from Mill, Salisbury, and Nottingham islands, Nunavut; Geological Survey of Canada, Current Research 2008-22, 17 p. doi:10.4095/226075

Rayner, N., Chakungal, J., and Sanborn-Barrie, M., 2011. New U-Pb geochronological results from plutonic and sedimentary rocks of Southampton Island, Nunavut; Geological Survey of Canada, Current Research 2011-5, 20 p. doi:10.4095/287286

Rayner, N.M., Moser, D.E., and Sanborn-Barrie, M., 2012. Speckled zircon from mafic granulite: mechanism and meaning; *in* Program with Abstracts, The 22nd V.M. Goldschmidt Conference, Montreal, Quebec; abstract no. 488.

Roddick, J.C., 1987. Generalized numerical error analysis with application to geochronology and thermodynamics; Geochimica et Cosmochimica Acta, v. 51, p. 2129–2135. doi:10.1016/0016-7037(87)90261-4

Sanborn-Barrie, M., Chakungal, J., James, D., Whalen, J., Berman, R.G., and Craven, J., 2007. The geology of Southampton Island, Nunavut, with a NE Laurentia Context; *in* 35th Annual Yellowknife Geoscience Forum Abstracts, (comp.) S. Cairns and S. Falck; YKGSF Abstracts Volume 2007, November 20–22, 2007, Northwest Territories Geoscience Office, Yellowknife, Northwest Territories, p. 54–55.

Sanborn-Barrie, M., Chakungal, J., James, D., Whalen, J., Rayner, N., Berman, R.G., Craven, J., and Coyle, M., 2008. New understanding of the geology and diamond prospectivity of Southampton Island, central Nunavut; *in* 36th Annual Yellowknife Geoscience Forum Abstracts, (comp.) V. Jackson and D. Irwin; YKGSF Abstracts Volume 2008, November 8–20, 2008, Northwest Territories Geoscience Office, Yellowknife, Northwest Territories, p. 53–54.

Sanborn-Barrie, M., Chakungal, J., and Buller, G., 2009. Bedrock field data and photographic record of exposed Precambrian basement, Southampton Island, Nunavut; Geological Survey of Canada, Open File 6177, 1 DVD. doi:10.4095/247890

Sanborn-Barrie, M., Chakungal, J., James, D.T., Rayner, N., and Whalen, J., in press. Precambrian bedrock geology, Southampton Island, Nunavut; Geological Survey of Canada, Canadian Geoscience Map 132, scale 1:250 000.

Stacey, J.S. and Kramers, J.D., 1975. Approximation of terrestrial lead isotope evolution by a two stage model; Earth and Planetary Science Letters, v. 26, p. 207–221. doi:10.1016/0012-821X(75)90088-6

Stauffer, M.R., 1984. Manikewan: an early Proterozoic ocean in central Canada, its igneous history and ocean closure; Precambrian Research, v. 25, p. 257–281. doi:10.1016/0301-9268(84)90036-6

Stern, R.A., 1997. The GSC Sensitive High Resolution Ion Microprobe (SHRIMP): analytical techniques of zircon U-Th-Pb age determinations and performance evaluation; *in* Radiogenic Age and Isotopic Studies, Report 10, Geological Survey of Canada, Current Research 1997-F, p. 1–31.

Stern, R.A., 2001. A new isotopic and trace-element standard for the ion microprobe: preliminary thermal ionization mass spectrometry (TIMS) U-Pb and electron-microprobe data; Radiogenic Age and Isotopic Studies, Report 14, Geological Survey of Canada, Current Research 2001-F1, 11 p. doi:10.4095/212668

Stern, R.A. and Amelin, Y., 2003. Assessment of errors in SIMS zircon U-Pb geochronology using a natural zircon standard and NIST SRM 610 glass; Chemical Geology, v. 197, p. 111–142. doi:10.1016/S0009-2541(02)00320-0

Sun, S.-s. and McDonough, W.F., 1989. Chemical and isotopic systematics of oceanic basalts: implications for mantle composition and processes; *in* Magmatism in the ocean basins, (ed.) A.D. Saunders and M.J. Norry; Geological Society of London, Special Publication no. 42, p. 313–345.

Whalen, J.B., Sanborn-Barrie, M., and Chakungal, J., 2011. Geochemical and Nd isotopic constraints from plutonic rocks on the magmatic and crustal evolution of Southampton Island, Nunavut; Geological Survey of Canada, Current Research 2011-2, 11 p. doi:10.4095/286319

Geological Survey of Canada Project MGM007